THE JOURNAL OF BIOLOGICAL CHEMISTRY
© 2004 by The American Society for Biochemistry and Molecular Biology, Inc.

Vol. 279, No. 30, Issue of July 23, pp. 30983–30993, 2004
Printed in U.S.A.

# Differentiation-dependent Sensitivity to Apoptogenic Factors in PC12 Cells*

Received for publication, January 21, 2004, and in revised form, May 7, 2004
Published, JBC Papers in Press, May 7, 2004, DOI 10.1074/jbc.M400692200

**Sheela Vyas‡§, Philippe Juin¶, David Hancock‖, Yasuyuki Suzuki**, Ryosuke Takahashi**, Antoine Triller‡, and Gerard Evan‡‡**

*From the ‡INSERM U497, Ecole Normale Supérieure, 46, rue d'Ulm, Paris 75005, ¶INSERM U419, 9 Quai Moncousu, 44035 Nantes Cedex, France, the ‖Signal Transduction Laboratory, Cancer Research UK, 44 Lincoln's Inn Fields, London WC2A 3PX, United Kingdom, the **Laboratory for Motor System Neurodegeneration, RIKEN Brain Science Institute, Saitama, 351-0198, Japan, and the ‡‡University of California at San Francisco Cancer Center, San Francisco, California 94143-0875*

**We have investigated the role of the mitochondrial pathway during cell death following serum and nerve growth factor (NGF)/dibutyryl cyclic AMP ($Bt_2$cAMP) withdrawal in undifferentiated or NGF/$Bt_2$cAMP-differentiated PC12 cells, respectively. Holocytochrome *c*, Smac/DIABLO, and Omi/HtrA2 are released rapidly following trophic factor deprivation in PC12 cells. Bcl-2 and Akt inhibited this release. The protection, however, persisted longer in differentiated PC12 cells. In differentiated, but not undifferentiated cells, Bcl-2 and Akt also inhibited apoptosis downstream of holocytochrome c release. Thus, undifferentiated PC12 cells showed marked sensitivity to induction of apoptosis by microinjected cytochrome *c* even in the presence of NGF, Bcl-2, or Akt. In contrast, in differentiated cells these factors suppressed cell death. Consistent with these observations, *in vitro* processing of procaspase 9 in response to cytochrome *c* was observed in extracts from undifferentiated but not differentiated cells expressing Akt or Bcl-2. Endogenous caspase 9 was cleaved during cell death, whereas dominant negative caspase 9 inhibited cell death. The results from determining the role of inhibitors of apoptosis (IAPs) suggest that acquisition of inhibition by IAPs is part of the differentiation program. Ubiquitin-ΔN-AVPI Smac/DIABLO induced cell death in differentiated cells only. c-IAP-2 is unregulated in differentiated cells, whereas X-linked IAP levels decreased in these cells coincident with cell death. Moreover, expressing X-linked IAP rendered undifferentiated cells resistant to microinjected cytochrome *c*. Overall, the inhibitory regulation, of cell death at the level of release of mitochondrial apoptogenic factors and at post-mitochondrial activation of caspase 9 observed in differentiated PC12 cells, is reduced or absent in the undifferentiated counterparts.**

Cell death is essential for the development of the nervous system, where neurogenic precursor cells are produced in excess and then eliminated at specified times during the migration and differentiation of distinct populations of neurons (1–3). Conversely, suppression of the cell death is vital for the maintenance of non-dividing neurons after terminal differentiation.

Compelling experimental evidence that apoptosis is critical for nervous system development has emerged from *in vivo* studies in mice carrying null mutations for various components of the apoptotic machinery such as *Bcl-$x_L$*, *caspases 3* and *9*, and *Apaf-1* genes (4–7). In all such cases, gross organizational anomalies in developing CNS contribute to the observed prenatal lethality. Thus, in the absence of *Bcl-$X_L$*, excessive death of differentiating neuronal cells occurs in brainstem and spinal cord. Embryonic mice with null mutations in *Apaf-1*, *caspase 3*, or *caspase 9* display morphological CNS abnormalities, as a result of supernumerary cells expanded ventricular zone and forebrain protrusions occur. The general inference from detailed analyses in such mice, as well as in the double knock-out mutant mice such as *Bcl-$x_L$*$^{-/-}$/*caspase 3*$^{-/-}$ and *Bcl-$x_L$*$^{-/-}$/*caspase 9* $^{-/-}$, is that cell death in CNS development not only serves to match the size of a neuronal population to its target field but is also vital for global morphogenesis of the nervous system. Additionally, such observations suggest that the mechanisms responsible for early cell death in neural progenitor cells may differ from those in post-mitotic neurons. In neural progenitor cells, caspase 3 or 9 function is independent of Bcl-$x_L$ regulation, whereas in post-mitotic neurons, Bcl-$x_L$ acts upstream of caspases 9 and 3 in an epistatic manner (8–10). Apoptotic pathways are also activated during inappropriate neuronal death that occurs in acute and chronic neurodegenerative diseases. For example, activated forms of caspases are observed in degenerating neurons following stroke and in Parkinson or Alzheimer diseases (11, 12).

Because caspases are the final implementers of apoptosis, tight control of caspase activation is crucial for long term survival of post-mitotic neurons. Caspases are synthesized as inactive zymogens that are catalytically activated by specific proteolytic cleavage, either by the action of upstream caspases or, in the case of the apical caspases, through autoactivation following their assembly into multimeric protein complexes (13–15). Mitochondria play a key role in orchestrating activation of one key apical caspase, caspase 9. In response to many mechanistically diverse pro-apoptotic triggers, mitochondria release multiple pro-apoptotic effectors from their inter-membrane space. One of these is holocytochrome *c* (hcC),[1] which, once in the cytosol, forms a complex with and activates the Apaf-1-caspase-9 holoenzyme to generate an active "apopto-

* This work was supported by an INSERM/Medical Research Council travel fellowship (to S. V.) and by the Association Francaise contre les Myopathies and Institut pour la Recherche sur la Moelle Epinière. The costs of publication of this article were defrayed in part by the payment of page charges. This article must therefore be hereby marked "*advertisement*" in accordance with 18 U.S.C. Section 1734 solely to indicate this fact.

§ To whom correspondence should be addressed. Tel.: 33-1-44-32-35-33; Fax: 33-1-44-32-36-54; E-mail: vyas@wotan.ens.fr.

[1] The abbreviations used are: hcC, holocytochrome *c*; NGF, nerve growth factor; $Bt_2$cAMP, dibutyryl cyclic AMP; PBS, phosphate-buffered saline; GFP, green fluorescent protein; Ub, ubiquitin; IAP, inhibitor of apoptosis; XIAP, X-linked IAP; Smac, second mitochondrial derived activator of caspases.

some" (16). Upon receipt of an apoptotic signal, mitochondria synchronously release all of their cytochrome *c* (17), although the exact molecular mechanism of its translocation remains unresolved (18–20). Several other apoptogenic factors are also released from mitochondria during cell death, among them Smac/DIABLO and Omi/HtrA2, which both act by binding to and inhibiting IAP function, releasing the activities of caspases 9, 3, and 7 (21–23). Substantial experimental evidence indicates that pro-apoptotic Bcl-2 family members such as Bax, Bak, and Bad promote hcC release and, therefore, trigger cell death, whereas the anti-apoptotic members Bcl-2 and Bcl-$x_L$ prevent cell death by inhibiting hcC release. In addition, exogenous survival factors such as NGF and insulin-like growth factor-1 inhibit cytochrome *c* release, in part through an Akt-dependent phosphorylation and deactivation of Bad (24, 25).

Non-differentiated, proliferating PC12 (pheochromocytoma) cells undergo cell death upon withdrawal of serum. However, they can be rescued by acute treatment with various survival factors such as insulin-like growth factor-1 or NGF or by administration of $Bt_2$cAMP (26, 27). In addition to signaling survival, some of these factors also induce differentiation of PC12 cells, although any mechanistic relationship between survival and differentiation is unclear. Although caspase-mediated cell death following withdrawal of serum or NGF in PC12 cells and in primary sympathetic neurons has been well studied (28–30), whether differentiation has a role in regulation of caspases has not been analyzed.

We have previously shown that NGF/$Bt_2$cAMP-induced differentiation leads to these cells becoming terminally and irreversibly differentiated, and, upon withdrawal of NGF and $Bt_2$cAMP, they die asynchronously by apoptosis (26). In this study, we have investigated the role of cytochrome *c*/caspase 9 activation during cell death induced by trophic factor withdrawal in undifferentiated and NGF/$Bt_2$cAMP-differentiated PC12 cells. In addition, the regulation of this cell death pathway by the pro-survival effectors Akt and Bcl-2 was examined.

## EXPERIMENTAL PROCEDURES

*Cell Culture and Preparation of Stably Expressing Cell Lines*—Undifferentiated PC12 cells were cultivated in RPMI 1640 medium containing 10% fetal calf serum and 5% horse serum. They were induced to differentiate in modified L15 medium containing 5% fetal calf serum, 10% horse serum, and 50 ng/ml NGF (7S form, Roche Applied Science) as previously described (26). After 3 days, 200 μM $Bt_2$cAMP (Sigma) was added, and the cells were differentiated for a further 4–5 days. Cell death was induced in undifferentiated cells (50–60% confluent) by serum withdrawal for 24–48 h. In differentiated cells, apoptosis was triggered by removal of NGF/$Bt_2$cAMP from the medium.

*Hbcl-2* (human *bcl-2*) cDNA inserted in pRc/CMV expression vector was electroporated into PC12 cells, G418-resistant hBcl-2 clones were selected, and expression of hBcl-2 protein was verified by Western blot analysis. DNA comprising *v-Akt-gag* inserted into the pLXSN vector was transfected into the GP+E packaging cell line, and ecotropic virus-containing supernatant was harvested and filtered. PC12 cells were treated for 5 h with this virus supernatant containing 8 μg/ml Polybrene. The virus supernatant was then replaced with RPMI/serum medium, and 24 h later the cells were selected in G418 (250 μg/ml) for a further 3 weeks, after which individual colonies were used for further analyses. cDNA encoding the dominant negative caspase 9 C287S point mutant fused to the FLAG epitope (C9DN) (31) was inserted into pcDNA3.1 vector and transfected into PC12 cells by LipofectAMINE treatment, and the G418-resistant pools of clones were selected. Expression of C9DN was verified by immunoblot analysis. G418-resistant PC12 cells in the presence of doxycycline (Sigma, 0.5 μg/ml) transfected with cDNA encoding for mouse XIAP in pN-21 tetracycline-repressible vector, were selected for XIAP function in undifferentiated cells. Parallel cultures of cells were transfected with empty plasmid vector and used as controls (PC12/C).

*Microinjection*—Undifferentiated and differentiated PC12 cells were cultivated on glass-bottomed coverslip dishes (MatTek Corp.). Cytochrome *c* (Sigma) solution was freshly prepared at desired concentrations and then mixed thoroughly with 0.4% (final concentration) rhodamine-dextran (Sigma), a fluorescent marker. In differentiated cells, where appropriate NGF/$Bt_2$cAMP was withdrawn just prior to microinjections. Doxycycline was withdrawn ~16 h prior to microinjections of XIAP/PC12 cells. After microinjections, the medium was replaced and cell death monitored at timed intervals. Microinjection parameters were kept constant: an automated Eppendorf microinjection system was used in which the pressure was held at 120 heptopascals and time at 0.2 s. Approximately 200–350 cells were microinjected for each study, and culture medium was replaced immediately after microinjections. Viability of microinjected cells was monitored by direct fluorescent microscopy at various time points. At high (×63 or ×100) magnification, rhodamine fluorescence was easily detectable in the cytoplasm and neurites of differentiated cells but excluded from the nuclei. The characteristic morphology of apoptosis, rounding up of cells accompanied by homogenous distribution of the rhodamine marker and fragmentation of nuclei and/or cytoplasm into apoptotic bodies, allowed us to quantify the apoptotic *versus* viable cells.

*Transient Transfections*—Undifferentiated and differentiated PC12 cells, cultured in 4-well multidishes, were transfected with 0.2 μg of pEGFP plus 0.8 μg of Ub-ΔN-AVPI-Myc or Ub-ΔN-MVPI Smac/DIABLO-Myc cloned in pcDNA3, using LipofectAMINE 2000 (Invitrogen) according to the manufacturer's instructions. Medium containing LipofectAMINE 2000 was removed after 6 h and replaced with appropriate normal medium. 24 h post-transfection, the cells were deprived of trophic support for 8 or 24 h and after PBS wash, were fixed with 4% paraformaldehyde. The cells were treated with 1 μg/ml Hoescht, and cell death was quantified by counting apoptotic nuclei of GFP-positive cells. It was verified that GFP-positive cells also express Ub-ΔN-AVPI-Myc or Ub-ΔN-MVPI Smac/DIABLO-myc by immunofluorescence using 9E10 anti-myc antibody.

*Biochemical Methods*—Soluble cytoplasmic and membrane fractions were prepared as described previously (32). Briefly, both undifferentiated and differentiated PC12 cells were cultured in 15-cm culture dishes. Cells in culture dishes were rinsed twice using ice-cold phosphate-buffered saline (PBS). They were harvested by adding a small volume (100 μl) of cold sucrose-supplemented cell extract buffer (300 mM sucrose, 10 mM HEPES (pH 7.4), 5 mM $MgCl_2$, 5 mM EGTA, 1 mM dithiothreitol, 10 mM cytochalasin B, and 1 mM phenylmethylsulfonyl fluoride) to culture dishes, scraped, and pelleted. The pellets were resuspended in the above buffer, incubated on ice for 30 min, homogenized, and centrifuged at 14,000 × *g* for 15 min. The supernatants comprising the cytoplasmic/soluble fraction and pellets (heavy membrane fraction) were separated and stored at −80 °C. Total cell lysates were prepared, after PBS wash, by directly adding Laemmli buffer containing protease inhibitors to cells; the samples were boiled and centrifuged. Total protein was quantified by the method of Bradford. The antibodies used were cytochrome *c* (antibody at 1:1000 dilution; BD Pharmingen, clone 7H8.2C12), cytochrome oxidase IV (antibody at 1:1000 dilution, Molecular Probes), Smac/DIABLO (produced at ICR, antibody at 1:1500 dilution), Omi/HtrA2 (antibody at 1:1000 dilution (22)), caspase 9 (antibody at 1:1000 dilution, Stressgen), c-IAP-2 (antibody at 1:1000 dilution, Santa Cruz Biotechnology), and XIAP (antibody at 1:1000 dilution (22)). The Smac/DIABLO antibody was made against mature N-terminal region (Cancer Research, UK), and the specificity was verified by peptide block. For immunoblot assays, 14, 12, or 10% SDS-PAGE gels were loaded with lysates containing appropriate concentrations of total protein. After transfer to Immobilon P membrane and incubation with primary and secondary antibodies, the signals were developed using enhanced chemiluminescence kit (Amersham Biosciences).

*In Vitro Procaspase 9 Processing*—Procaspase 9 cDNA in pBluescript was *in vitro* transcribed with T3 RNA polymerase, translated, and radiolabeled with $^{35}$S-labeled methionine/cysteine (Amersham Biosciences) using the TnT-coupled transcription/translation rabbit reticulocyte lysate system (Promega). Processing of *in vitro*-translated procaspase 9 product by the cytoplasmic extracts prepared from PC12 cells was assayed essentially as described previously (31). Briefly, 1.5 μl of [$^{35}$S]procaspase 9 product was incubated at 30 °C for 30 min with cytoplasmic extracts containing 20 μg of protein (prepared as described above for hcC analysis) in the presence or absence of cytochrome *c* (10 mM) and dATP (1 mM): all in 10-ml total volume. Laemmli buffer was added, and the samples were boiled and fractionated by SDS-PAGE analysis followed by autoradiography.

## RESULTS

*Cytochrome c Release in Undifferentiated PC12 Cells following Withdrawal of Serum*—The kinetics of subcellular redistri-

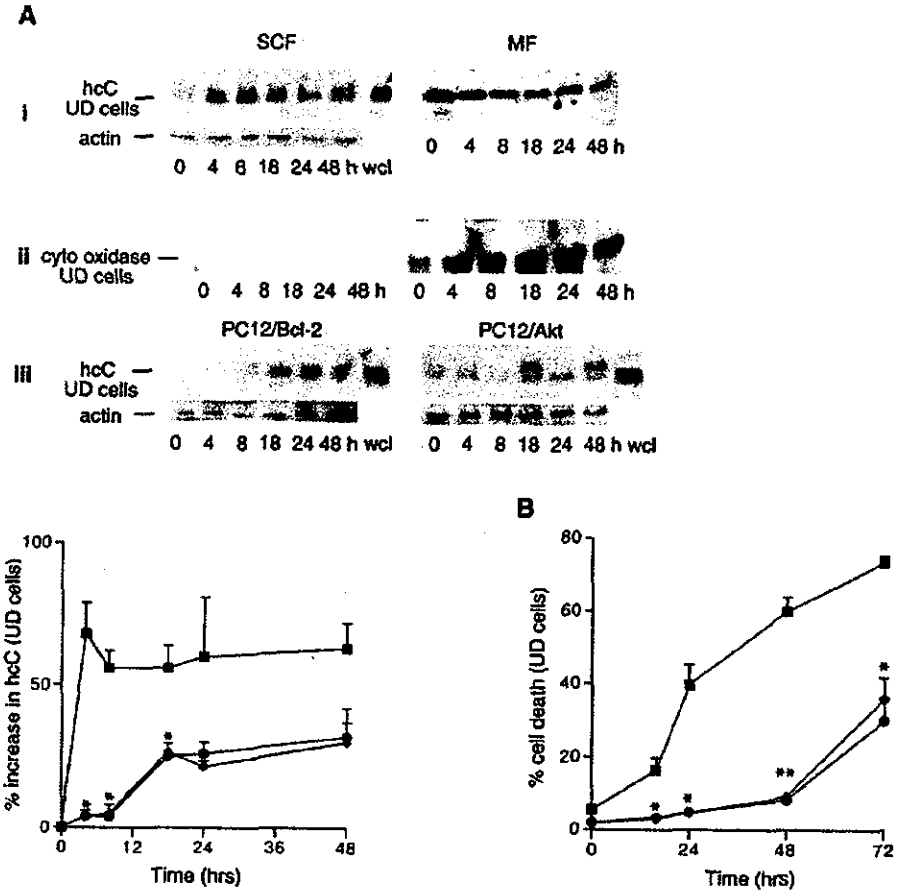


FIG. 1. **Kinetics of holocytochrome c (hcC) release and cell death in undifferentiated (*UD*) PC12 control (*PC12/C*), PC12/Bcl-2, and PC12/Akt cells.** *A*, soluble cytosolic fraction (*SCF*) and membrane fractions (*MF*) were prepared from serum containing 0, 4, 8, 18, 24, 36, and 48-h serum-deprived cells. An aliquot (whole cell lysate, *wcl*) was taken from serum-containing cells before fractionation and solubilized by adding 0.1% Triton X-100. 20 $\mu$g of total protein of SF and whole cell lysate (*wcl*) and 10 $\mu$g of MF was used for analysis of cytochrome *c* content. The autoradiograms of a representative experiment are shown. *i*, hcC in SCF and MF of PC12/C cells; *ii*, hcC immunoblot was stripped and reprobed with anti-cytochrome oxidase IV antibody; the protein is present only in MF; *iii*, hcC in SCF and wcl of PC12/Bcl-2 and PC12/Akt cells deprived of serum up to 48 h. The SCF blots were reprobed with actin as control for protein loading. The autoradiogram signals of SCF blots were densitometrically quantified (*bottom left panel*) using Gel Analyst software program. These results, which represent data from 3–5 experiments for each cell type: PC12/C (*solid square*), PC12/Bcl-2 (*solid diamond*), and PC12/Akt (*solid circle*), are expressed as % increase in hcC, mean ± S.E. using the 0 h value as control. *, $p$ value < 0.05, PC12/Bcl-2 or Akt *versus* PC12/C (Student's $t$ test, two-tailed). *B*, undifferentiated PC12/C (*solid square*), PC12/Bcl-2 (*solid diamond*), and PC12/Akt (*solid circle*) cells were deprived of serum for 18, 24, 48, and 72 h, fixed with 4% paraformaldehyde, and nuclei were stained with 1 $\mu$g/ml Hoechst 33258. Apoptotic nuclei were quantified by analyzing five random fields, each field comprising ~150 nuclei. Each time point was assayed in quadruplicate; the results are expressed as % mean ± S.E. of at least three experiments. $p$ values: 8, <0.05 and **, 0.01; PC12/Bcl-2 and Akt *versus* PC/12 cells (Student's $t$ test, two-tailed).

bution of hcC from mitochondria to cytosol in PC12 cells following withdrawal of trophic support was first analyzed. The amount of hcC in the membrane fraction containing intact mitochondria (verified by electron microscopy) *versus* the soluble cytoplasmic fraction was determined by immunoblotting. Proliferating undifferentiated PC12 cells maintained in high serum exhibited negligible cytoplasmic hcC. However, withdrawal of serum resulted in a rapid increase in cytosolic hcC, evident by 4 h and persisting at all the time points tested (Fig. 1*A*, *panel i*). In contrast to hcC, the integral mitochondrial protein, cytochrome oxidase IV was retained within the membrane fraction (Fig. 1*A*, *panel ii*). The cytosolic accumulation of hcC precedes cell death that begins around 18 h after serum deprivation (Fig. 1*B*).

Because Akt and Bcl-2 can suppress the release of hcC from mitochondria and inhibit apoptosis in several cell types (25, 33), we next assayed cytochrome *c* translocation following serum deprivation in PC12 cells constitutively expressing either active v-*Akt-gag* (PC12/Akt) or h*Bcl-2* (PC12/Bcl-2). Each study was conducted in two independent clones in which expression of either v-Akt-gag or hBcl-2 had been previously verified by immunoblotting (data not shown). In addition, the activated status of v-Akt-gag was confirmed with an antibody specific for phosphorylated Akt at Ser-473 (data not shown). The PC12/Akt and PC12/Bcl-2 clones used each expressed comparable levels of v-*Akt-gag* or h*Bcl-2*, respectively. During the 24- to 48-h time period of serum deprivation, expression of either v-*Akt-gag* or h*Bcl-2* significantly inhibited cell death in undifferentiated PC12 cells (Fig. 1*B*). For example, upon withdrawal of serum for 24 h, we observed 40 ± 5.5% cell death in control cells compared with <5% in either Akt- or Bcl-2-expressing clones. However, such protection was not absolute, because more extended 72-h serum deprivation elicited some 30% death in both PC12/Bcl-2 and PC12/Akt cells (compared with 80% in PC12 control cells) (Fig. 1*B*). Immunoblot analysis of hcC levels in serum-deprived PC12/Akt and PC12/Bcl-2 cells showed that cytoplasmic hcC levels only rise ~18 h after withdrawal of serum (Fig. 1*A*, *panel iii*). The quantification of signals revealed that the accumulation of hcC in cytoplasm of these cells was less than in control PC12 cells. Analysis of hcC in whole cell lysates showed comparable levels of hcC in PC12/control, PC12/Bcl-2, and PC12/Akt cells. Thus both Bcl-2 and Akt act to

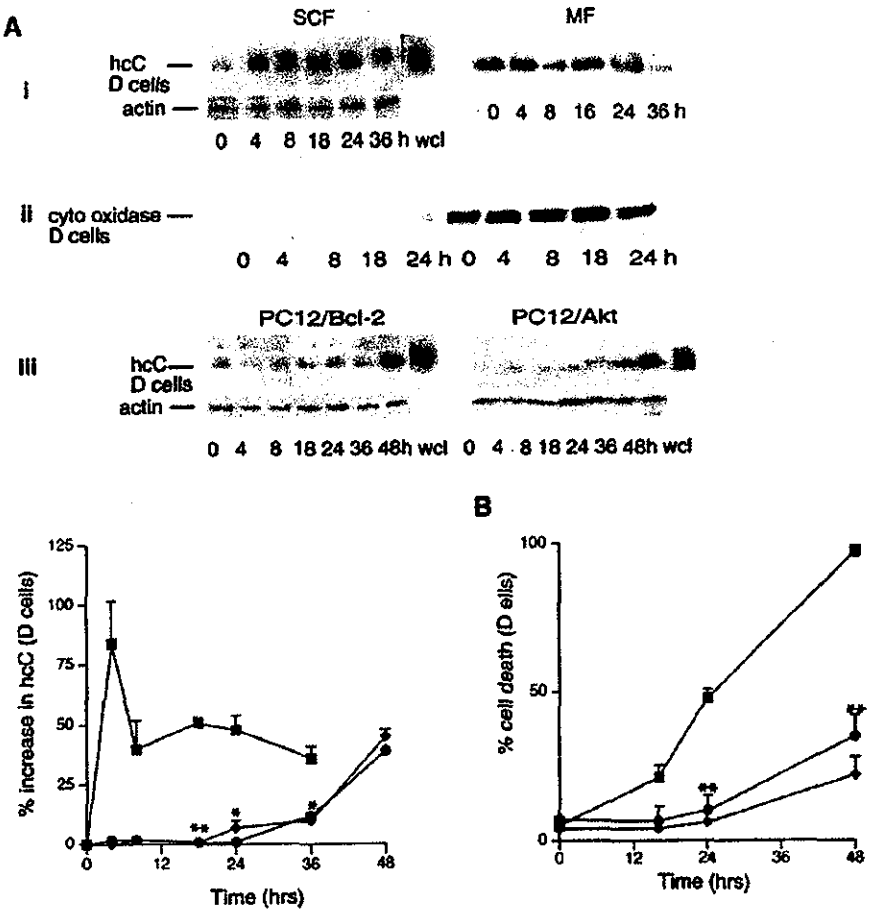


FIG. 2. **Holocytochrome c (hcC) release and cell death after withdrawal of NGF/$Bt_2$cAMP from NGF/$Bt_2$cAMP differentiated (*D*) PC12/C, PC12/Bcl-2, and PC12/Akt cells.** PC12 cells were differentiated with NGF/$Bt_2$cAMP followed by withdrawal of the latter at different times (h) as indicated. *A*, hcC content was analyzed in soluble cytosolic fraction (*SCF*) and membrane fraction (*MF*) at different times following NGF/$Bt_2$cAMP withdrawal. 20 $\mu$g of total protein of SCF and whole cell lysate (*wcl*) and 10 $\mu$g of MF were used for immunoblot assays. Results of a representative experiment of hcC content are shown in the *left panel*: *i*, hcC protein content in SCF, wcl, and MF of differentiated PC12/C cells (0) deprived of NGF/$Bt_2$cAMP for up to 36 h; *ii*, hcC immunoblot was stripped and reprobed for cytochrome *c* oxidase IV, which was present only in the MF; *iii*, hcC content in SCF of differentiated PC12/Bcl-2 and PC12/Akt cells (0 h) deprived of NGF/$Bt_2$cAMP for up to 48 h. Results of actin as control for protein loading are shown at the *bottom*. hcC in SCF was quantified (*bottom left panel*), the results are expressed as % increase in hcC, mean ± S.E. using 0 h value as control ($n = 4$). $p$ values: *, <0.05; **, 0.01; PC12/Bcl-2 or Akt *versus* PC12/C cells (Student's $t$ test, two-tailed). *B*, the kinetics of cell death was analyzed in differentiated PC12/C (*solid square*), PC12/Bcl-2 (*solid diamond*), and PC12/Akt (*solid circle*) cells following deprivation of NGF/$Bt_2$cAMP for up to 48 h. The cells were stained with 1 $\mu$g/ml Hoechst 33258, and the apoptotic nuclei were quantified. The results are expressed as % mean ± S.E. of three independent experiments. **, $p < 0.01$; PC12/Bcl-2 or Akt *versus* PC12/C cells (Student's $t$ test, two-tailed).

inhibit and delay the otherwise rapid translocation of hcC observed in control PC12 cells.

Immunocytochemical staining for hcC corroborated the above immunoblot analysis. PC12 control (PC12/C), PC12/Bcl-2, and PC12/Akt cells in the presence of serum showed punctate mitochondrial hcC staining evident as a rim around the nucleus. In contrast, serum deprivation of PC12/C for as little as 8 h resulted in many cells showing diffuse cytosolic hcC labeling that persisted throughout the period of serum deprivation. PC12/Bcl-2 and PC12/Akt cells deprived of serum for 8 h retained a punctate mitochondrial hcC distribution, which nonetheless became diffuse and cytosolic after 24-h deprivation (data not shown).

*Cytochrome c Release in Differentiated PC12 Cells following Withdrawal of NGF/$Bt_2$cAMP*—Like their undifferentiated counterparts, differentiated PC12 cells deprived of NGF and $Bt_2$cAMP also showed cytosolic hcC, which was evident by 4 h of deprivation, and persisted to 48 h (Fig. 2*A*, *panel i*), in contrast cytochrome oxidase IV was observed only within the membrane fraction (Fig. 2*A*, *panel ii*). Again, the release of hcC precedes cell death (Fig. 2*B*). Release of hcC from mitochondria was confirmed by immunocytochemical staining of equivalent cells, which showed that control differentiated PC12 cells retained punctate somatic and neuritic staining, whereas diffuse hcC staining was already evident in some cells by 4–6 h following deprivation of NGF/$Bt_2$cAMP. By 24 h of factor deprivation, many cells displayed both diffuse hcC cytoplasmic pattern and nuclear morphology characteristic of apoptosis (data not shown).

In undifferentiated PC12 cells, as described above, both Bcl-2 and Akt delayed hcC translocation to cytoplasm for ~18 h. No significant increase in cytosolic hcC was observed until 48 h in either differentiated PC12/Bcl-2 or PC12/Akt cells deprived of NGF/$Bt_2$cAMP (Fig. 2*A*, *panel iii*). 48 h after withdrawal of NGF/$Bt_2$cAMP, about 20% of cell death was observed in these cells (Fig. 2*B*). Immunocytochemical analysis revealed a punctate mitochondrial distribution of hcC in cell soma and neurites in 24 h factor-deprived cells that was similar to that in undeprived control cells (data not shown). Overall these results indicate that expression of either Bcl-2 or Akt in factor-deprived differentiated PC12 cells suppresses hcC release and this for a longer period than in factor-deprived undifferentiated cells.

*Undifferentiated and Differentiated PC12 Cells Display Different Sensitivities to Microinjected Cytochrome c*—Release of hcC implies a role of caspase 9 (and caspase 3) pathway during trophic factor deprivation. To clarify any role increased cytosolic hcC might have in PC12 cell death, undifferentiated (proliferating) and differentiated PC12 cells were each microinjected with holocytochrome *c* together with dextran-conjugated rhodamine as a fluorescent marker. In parallel experiments, the same number of cells was microinjected with dextran-rhodamine marker alone as a control for trauma from microinjections. Subsequent cell fate was then followed after various times by fluorescence microscopy. In both undifferentiated and differentiated PC12 cells, apoptosis was induced, and its extent, dependent on the dose of cytochrome *c*. However, undifferentiated cells were far more sensitive to induction of apoptosis by a given dose of microinjected cytochrome *c*. Thus, at 2 h, 40% of the injected undifferentiated cells (10 $\mu$M cytochrome *c*) had died, whereas there was no significant increase in the percentage of cell death in the differentiated population. However, by

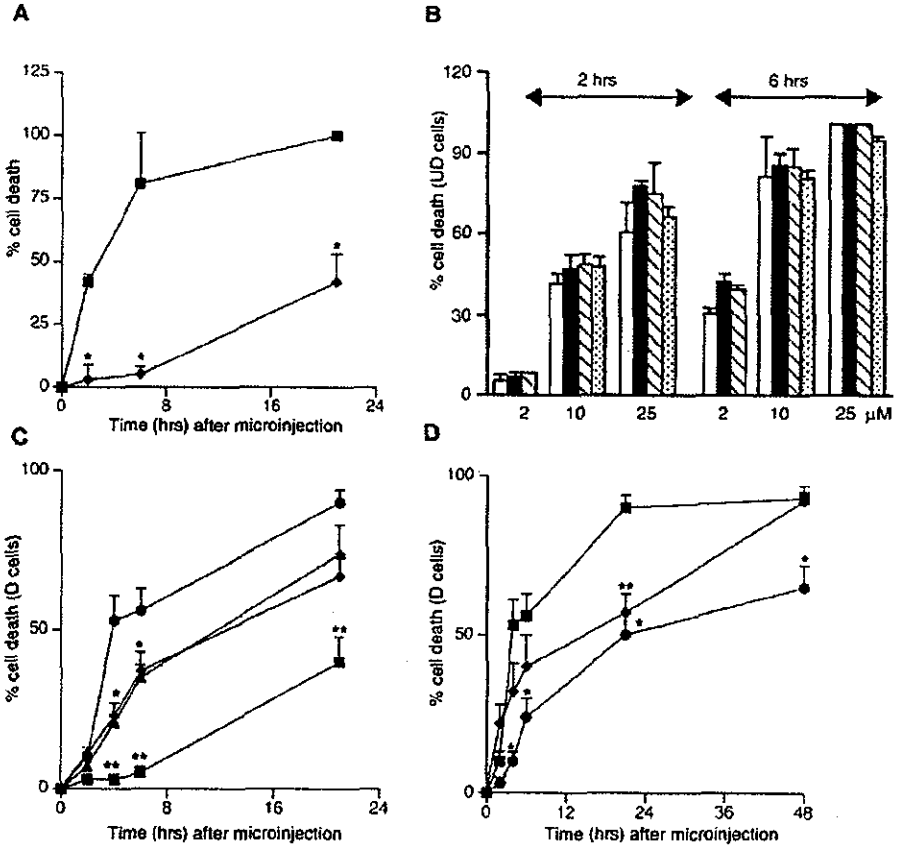


FIG. 3. **Cell death in undifferentiated and differentiated PC12 cells following cytochrome *c* microinjection.** *A*, differentiation-dependent sensitivity to microinjected cytochrome *c* (10 μM) in undifferentiated, serum-containing PC12 cells (*solid square*) and in NGF/$Bt_2$cAMP-differentiated PC12 cells (*solid diamond*). Cell death was quantified by counting rhodamine-positive viable and apoptotic cells at the times indicated. The results are presented as mean ± S.E. ($n$ = 3 for undifferentiated cells and 6 for differentiated cells). *, $p < 0.05$; differentiated *versus* undifferentiated cells. *B*, different concentrations of cytochrome *c* (indicated at the *bottom*) were microinjected in undifferentiated PC12/C (*open square*), PC12/Bcl-2 (*solid square*), PC12/Akt (*square* with *bar*), or PC12/C cells treated for 24 h with NGF (100 ng/ml) (*square* with *dots*). Cell death was quantified 2 and 6 h after microinjections. The results represent mean ± S.E. of three experiments done in duplicates. *C*, the consequences of 10 μM cytochrome *c* microinjection on cell death were assessed in differentiated (*D*) PC12/C cells, either in the presence of NGF/$Bt_2$cAMP (*solid square*) or in the absence of NGF/$Bt_2$cAMP (*solid circle*). In parallel, differentiated PC12 cells deprived of NGF/$Bt_2$cAMP were also microinjected with rhodamine only, as control for microinjection-induced cell death (*solid diamond*). NGF/$Bt_2$cAMP-differentiated PC12 cells were pre-treated with benzyloxycarbonyl-VAD-fluoromethyl ketone (10 μM) for 4 h prior to cytochrome *c* microinjections (*solid triangle*). After microinjections, cell death was quantified at the times indicated by fluorescence microscopy. The results are presented as mean ± S.E. of four to six experiments. *, $p < 0.005$; cytochrome *c*-microinjected death in NGF/$Bt_2$cAMP-deprived cells at 4 and 6 h in cells in benzyloxycarbonyl-VAD-treated *versus* NGF/$Bt_2$cAMP-deprived non-treated cells. **, $p < 0.05$; cytochrome *c*-microinjected death in NGF/$Bt_2$cAMP-containing cells at 4, 6, and 21 h *versus* cell death in NGF/$Bt_2$cAMP-deprived cells (Student's *t* test, two-tailed). *D*, protection by Bcl-2 and Akt in differentiated (*D*) PC12/Bcl-2 (*solid circle*) and PC12/Akt cells (*solid diamond*) deprived of NGF/$Bt_2$cAMP and microinjected with 10 μM cytochrome *c*. Results of PC12/C (*solid square*) are also shown. Cell death was analyzed at different time points after microinjections, up to 48 h. The results are presented as mean ± S.E. of three to five experiments. *, $p < 0.05$, in cytochrome *c*-microinjected PC12/Bcl-2 cells *versus* PC12/C cells at 4, 6, 21, and 48 h. *, $p < 0.05$; in cytochrome *c*-microinjected PC12/Akt *versus* PC12/C cells at 21 h (Student's *t* test, two-tailed).

21 h, some 42% of microinjected differentiated PC12 cells had died, indicating that cytochrome c was eventually pro-apoptotic, albeit with greatly delayed kinetics (Fig. 3*A*). This differential sensitivity to microinjected hcC was also observed in cells microinjected with the higher concentration (25 μM) of cytochrome *c*, although with more rapid cell death kinetics in both undifferentiated and differentiated cells (data not shown), confirming that cytochrome *c*-induced cell death is dose-dependent. These data are consistent with the notion that differentiated PC12 cells, unlike their undifferentiated counterparts, can to some extent be protected by intracellular signals capable of ameliorating cell survival even in the presence of exogenous cytochrome *c*.

We next analyzed whether NGF, Bcl-2, or Akt inhibit cell death induced by microinjected holocytochrome c in either undifferentiated or differentiated PC12 cells. Interestingly, in undifferentiated PC12 cells, none of these factors exerted any measurable inhibitory effect on cell death kinetics analyzed 2 and 6 h following microinjections of 2, 10, and 25 μM concentrations of cytochrome *c* (Fig. 3*B*). In contrast, in differentiated PC12 cells, cell death induced by microinjection of 10 μM cytochrome *c* was significantly ameliorated by NGF/$Bt_2$cAMP: for example, 42 ± 10% NGF/$Bt_2$cAMP-treated cells died compared with 91 ± 4% dead cells in similarly microinjected cells deprived of NGF/$Bt_2$cAMP (Fig. 3*C*). Although withdrawal of NGF/$Bt_2$cAMP from differentiated PC12 cells alone leads to some cell death, this is significantly less than that observed following microinjection of cytochrome *c* (23 ± 2% control cells dead at 4 h *versus* 54 ± 8% cells microinjected with cytochrome *c*). These data indicate that increasing cytosolic cytochrome *c* in the absence of survival factors accelerates cell death in differentiated cells (Fig. 3*C*). Pre-treatment of trophic-deprived cells with the broad-specificity caspase inhibitor, benzyloxycarbonyl-VAD-fluoromethyl ketone (10 μM) inhibited, although not completely, apoptosis induced by cytochrome *c* microinjections (Fig. 3*C*), in accordance with previous reports that caspases act downstream in cytochrome *c*-mediated cell death. In sharp contrast to undifferentiated cells, we observed that

Bcl-2 and Akt suppressed cell death in differentiated PC12 cells that were deprived of NGF/$Bt_2$cAMP and immediately microinjected with 10 μM cytochrome *c* (Fig. 3*D*). Taken together, our results show first that sensitivity to cytosolic cytochrome *c* decreases during PC12 cell differentiation and second that in differentiated but not undifferentiated PC12 cells, Akt and Bcl-2 can suppress apoptosis downstream of cytosolic hcC.

*Caspase 9 Activation Is Also Differentially Regulated between Undifferentiated and Differentiated PC12 Cells*—One potential implication of our findings is that NGF/$Bt_2$cAMP signaling regulates cell death downstream of cytochrome *c* release, possibly at the level of activation of caspase 9. To investigate this, we next examined the abilities of extracts derived from factor-deprived PC12 cells to induce cleavage and activation of *in vitro* translated procaspase 9. Procaspase 9 is cleaved into a detectable large subunit of either 35 or 37 kDa depending on the cleavage site Asp-315 or Asp-330. Processing at Asp-330 resulting in the p37 fragment is also triggered by activated caspase 3 (31).

Incubation of cytoplasmic extracts without cytochrome *c* and dATP does not result in the autocatalytic activity of procaspase 9 (Fig. 4*A*, compare *panels a* and *b*). Only cytoplasmic extracts (soluble fraction) and not microsomal fractions prepared from trophic factor-deprived PC12 cells triggered cleavage of procaspase 9 with concomitant appearance of the signature 37- and 35-kDa large caspase 9 fragments (Fig. 4*A*, *panel c*).

No procaspase 9 cleavage was induced, in the presence of exogenous cytochrome *c*/dATP, by cytosolic extracts from NGF/$Bt_2$cAMP-differentiated cells maintained in NGF/$Bt_2$cAMP: in contrast, analogous extracts derived from differentiated PC12 cells deprived of NGF/$Bt_2$cAMP for 24 h triggered cleavage of the majority of procaspase 9 (Fig. 4*B*). Pre-treatment of apoptotic lysates of cells with caspase 3 inhibitor Acetyl-Asp-Glu-Val-Asp-aldehyde (Ac-DEVD-CHO) completely blocked *in vitro* processing of procaspase 9 (Fig. 4, *B* and *C*). Thus, processing of procaspase 9 is specific for cytosolic extracts from factor-deprived cells and requires DEVD-specific caspase activity. Because expression of either Bcl-2 or activated Akt suppresses apoptosis in cytochrome *c*-microinjected differentiated PC12 cells, we asked whether extracts from such cells are able to induce procaspase 9 cleavage. Indeed, as shown in Fig. 4*B*, cell extracts from factor-deprived PC12 cells expressing either Bcl-2 or activated Akt, with added cytochrome *c*/dATP exhibited no procaspase 9 cleaving activity, suggesting that Bcl-2 and Akt expression also causes modification of caspase 9 activity of these extracts.

Procaspase 9 was also not processed in the presence of cytoplasmic extracts prepared from proliferating undifferentiated PC12 cells, following addition of cytochrome *c*/dATP, but was rapidly processed by extracts from serum-deprived cells (Fig. 4*C*). Furthermore, extracts from serum-deprived PC12 cells expressing either Bcl-2 or activated-Akt were equally effective at triggering procaspase 9 processing, indicating that these factors are not exercising controls on procaspase 9 cleavage to inhibit cell death.

To confirm the critical role for caspase 9 in determining death of PC12 cells, first the processing of endogenous procaspase 9, during the withdrawal of trophic support, was verified both in undifferentiated and differentiated cells. The 37-kDa cleavage product of procaspase 9 was seen only in trophic-deprived lysates strongly indicating its potential role in cell death (Fig. 4, *D* and *E*). Because processing of caspase 9 may not necessarily signify that it is catalytically active (34), we transfected PC12 cells with a cDNA encoding a dominant negative procaspase 9 (C9DN) that has a mutation in its active site (C287S) and has been shown to block cell death (35). PC12 cells stably expressing C9DN were prepared, and the kinetics of apoptosis in both undifferentiated and NGF/$Bt_2$cAMP-differentiated cells was examined. Cell death induced by serum deprivation for 24 h was significantly inhibited in undifferentiated PC12/C9DN cells compared with controls (Fig. 4*F*). In addition, apoptosis of differentiated PC12 cells expressing C9DN and deprived of NGF/$Bt_2$cAMP for 24 h was significantly retarded (Fig. 4*G*) indicating the importance of caspase 9 for this process.

*Smac/DIABLO and Omi/HtrA2 Are Also Released from Mitochondria of PC12 Cells Deprived of Trophic Support*—Recent biochemical and structural studies have revealed not only how some IAP family members inhibit proteolytic activities of initiator (caspase 9) and effector caspases (caspase 3 and 7) but also the mechanism by which this inhibition is effectively eliminated during cell death by mitochondrial proteins such as Smac/DIABLO and Omi/HtrA2 (34, 36). Through their BIR (baculoviral IAP repeat) domains, IAPs bind and inhibit the catalytic activity of processed forms caspases 9, 3, and 7. The mature forms of Smac/DIABLO and Omi/HtrA2, containing an exposed IAP binding motif (IBM), once released from mitochondria promote apoptosis by binding to IAPs and relieving caspase inhibition. To determine whether the differential sensitivity to cytochrome *c* that we observe between undifferentiated and differentiated cells could be related to the mechanism of IAP regulation of caspases, we first examined the release of Smac/DIABLO and Omi/HtrA2 from mitochondria. Withdrawal of serum or NGF/$Bt_2$cAMP from control undifferentiated or differentiated PC12 cells, respectively, resulted in increased cytosolic levels of Smac/DIABLO and Omi/HtrA2, with kinetics similar to hcC release (Fig. 5, *A*, *panel i*, *B*, *panel i*, and *C*, *panels i* and *ii*). The effect of Bcl-2 and Akt on translocation of Smac/DIABLO in factor-deprived cells was also analyzed. Deprivation of serum in undifferentiated PC12/Bcl-2 and PC12/Akt cells resulted in delayed cytoplasmic accumulation of Smac/DIABLO (at around 18 h) (Fig. 5*A*, *panels ii* and *iii*), although the results of quantification showed that, like hcC, the amount released at 18 h was less than that seen in control cells. In contrast, in NGF/$Bt_2$cAMP-deprived PC12/Bcl-2 or PC12/Akt-differentiated cells, cytoplasmic accumulation of these proteins was not observed even at 24 h (Fig. 5*B*, *panels ii* and *iii*). These results suggest that Bcl-2 and Akt co-regulate the release of hcC together with other pro-apoptotic factors from mitochondria during withdrawal of trophic support.

*Differentiated but Not Undifferentiated PC12 Cells Are Sensitive to Active Smac/DIABLO*—Proteolytic processing of Smac/DIABLO or Omi/HtrA2 results in the removal of mitochondrial signal peptide sequence and exposure of a novel N termini or IBM containing the tetrapeptide sequence AVPI, which has been shown to bind to IAPs (37, 38). To elucidate whether cytochrome *c* sensitivity of caspase 9 pathway is dependent on AVPI proteins, undifferentiated and differentiated PC12 cells were transiently co-transfected with plasmids encoding cDNAs for GFP and ubiquitin (Ub) fused to ΔN-AVPI Smac/DIABLO or the inactive Ub-ΔN-MVPI Smac/DIABLO. Intracellular processing of ubiquitin has been shown to yield mature Smac/DIABLO protein with exposed tetrapeptide sequence (39). Cell death was monitored and quantified by counting Hoescht stained apoptotic nuclei of GFP-positive cells, at 8 and 24 h following withdrawal of trophic support. In undifferentiated PC12/C cells, following withdrawal of serum, increased cell death was observed at 8 and 24 h; however, there was no difference in cultures transfected with Ub-ΔN-AVPI or MVPI-smac/DIABLO. There was some cell death at 8 h in control cells, which may be due to other regions than N-terminal of Smac/DIABLO-sensitizing serum-deprived cells to apoptosis (40) (Fig. 6*A*). Transfection of Ub-ΔN-AVPI-smac/DIABLO in

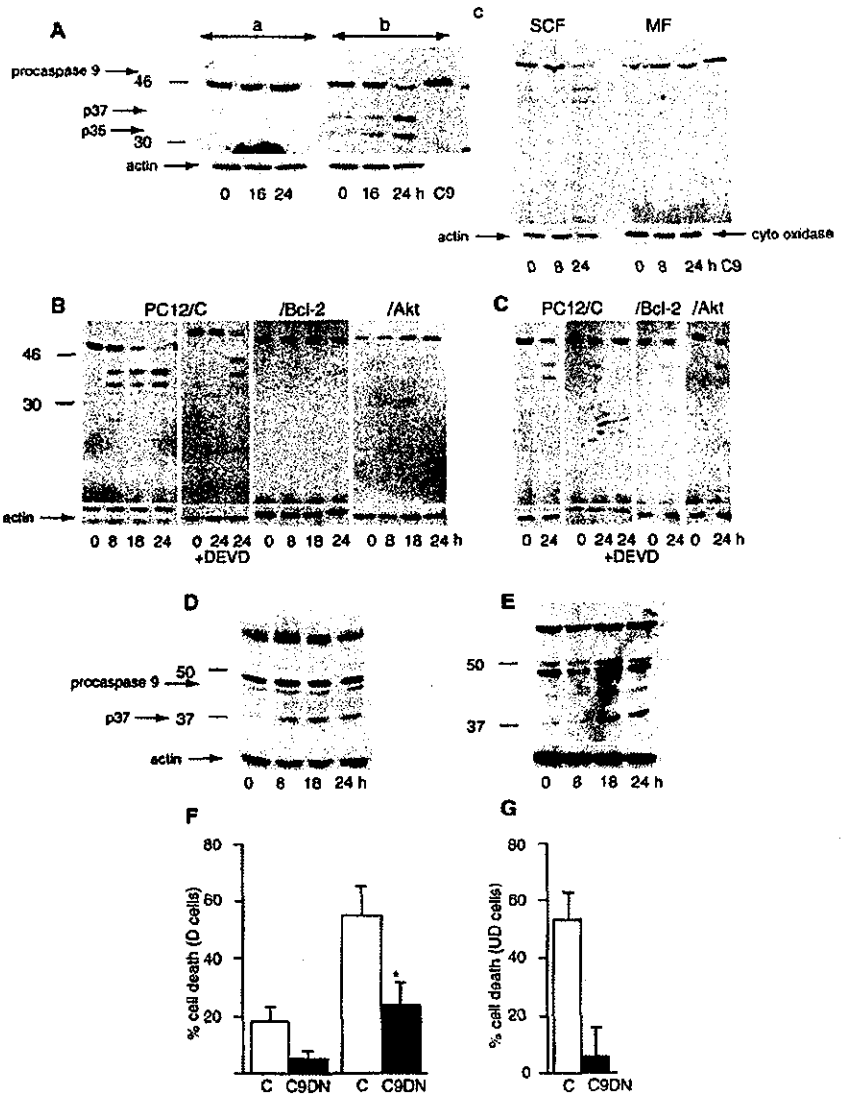


FIG. 4. **Regulation and role of caspase 9 in cell death of trophic support deprived PC12 cells.** *A*, $^{35}$S-labeled procaspase 9 processing by cytosolic extracts prepared from differentiated PC12 cells deprived of NGF/$Bt_2$cAMP for 16 and 24 h in the absence (*a*) and presence (*b*) of 10 mM cytochrome *c* and 1 mM dATP. Processing of *in vitro* labeled procaspase 9 was analyzed in membrane (*MF*) and in soluble cytosolic fractions (*SCF*) in the presence of cytochrome *c*/dATP (*c*). An aliquot (1.5 $\mu$l) of *in vitro* translated procaspase 9 product is shown in the last lane (*C9*). Shown also are the results of actin and cytochrome oxidase as protein controls of the SCF and MF lysates, respectively, used in the reaction. These controls were done separately using the same lysates and the same amount of total protein (20 $\mu$g). *B*, kinetics of procaspase 9 processing in differentiated PC12/C cells deprived of NGF/$Bt_2$cAMP. Cytoplasmic lysates were prepared at times indicated after withdrawal of NGF/$Bt_2$cAMP. Addition of caspase inhibitor Ac-DEVD-CHO inhibits procaspase 9 processing in extracts from differentiated PC12/C cells deprived of NGF/$Bt_2$cAMP for 24 h. Procaspase 9 is not processed in lysates prepared from differentiated PC12/Bcl-2 cells or PC12/Akt cells. NGF/$Bt_2$cAMP was withdrawn from these cells at times indicated. Results of actin as control for lysates used are shown below. *C*, procaspase 9 processing in undifferentiated PC12 cells containing serum (0) and following serum deprivation for 24 h that stimulates the processing, which was not prevented in PC12/Bcl-2 or PC12/Akt cells. However, prior Ac-DEVD-CHO treatment inhibited caspase 9 processing. Actin control is shown below. *D* and *E*, endogenous cleavage of caspase 9 following withdrawal of trophic support from differentiated (*D*) and undifferentiated (*E*) cells. The anti-caspase 9 antibody recognized procaspase 9 and the p37 large subunit, which is evident in trophic factor-deprived lysates. The bots were probed with anti-actin antibody as control for protein loading. *F* and *G*, inhibition of cell death in PC12 cells expressing dominant negative caspase 9 (*PC12/C9DN*). Cell death, in the presence of trophic support, time 0 h, in undifferentiated and differentiated cells in PC12/C and PC12/caspase 9 DN is 4–5 ± 2% (mean ± S.E.). *F*, differentiated (*D*) PC12/C and PC12/C9DN were deprived of NGF/$Bt_2$cAMP for 16 and 21 h ($n$ = 4). Apoptotic cells were quantified after staining with 1 $\mu$g/ml Hoechst 33258. *, $p < 0.05$; cell death in control *versus* in C9 dominant negative cells. *G*, undifferentiated (*UD*) cells were deprived of serum for 24 h. The results are presented as mean ± S.D. ($n$ = 3).

factor-deprived undifferentiated PC12/Bcl-2 or PC12/Akt cells did not result in significantly more cell death compared with cells transfected with Ub-ΔN-MVPI Smac/DIABLO (Fig. 6*A*). In contrast, NGF/$Bt_2$cAMP-deprived control, Bcl-2-expressing, or Akt-expressing differentiated PC12 cells were susceptible to cell death by Ub-ΔN-AVPI Smac/DIABLO but not Ub-ΔN-MVPI Smac/DIABLO (Fig. 6*B*). Increased cell death in PC12/C-differentiated cells was seen even in the presence of NGF/$Bt_2$cAMP. These results suggest that, although IBM of Smac/DIABLO is not required for cell death by trophic factor deprivation in undifferentiated cells, it plays an important role in regulating caspase activation in differentiated cells. Further, the anti-apoptotic function of Bcl-2 and Akt is antagonized by Ub-ΔN-AVPI Smac/DIABLO in differentiated cells indicating that inhibition of Smac/DIABLO release by Bcl-2 or Akt is crucial to suppressing cell death.

*Role of IAPs in Regulating Cell Death in Undifferentiated and Differentiated PC12 Cells*—The above results strongly indicate that the release of mitochondrial proteins Smac/DIABLO and Omi/HtrA2 that act to relieve IAP inhibition of

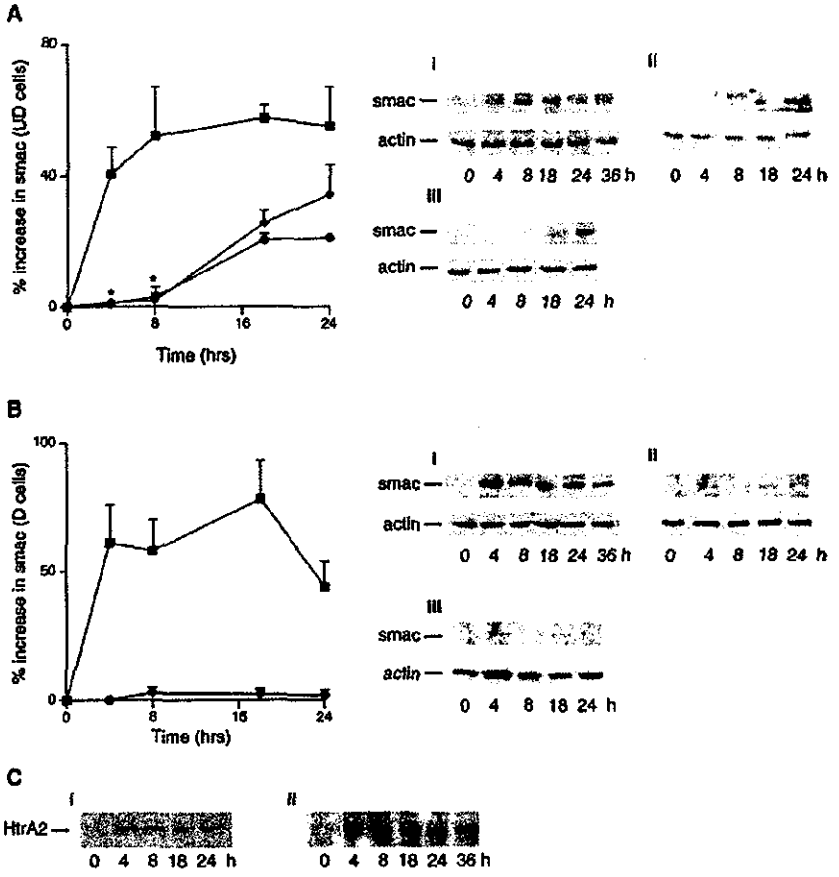


FIG. 5. **Immunoblot analysis of Smac/DIABLO and omi/HtrA2 levels in undifferentiated and NGF/$Bt_2$cAMP-differentiated PC12 cells following trophic factor deprivation.** *A*, for immunoblot analysis of Smac/DIABLO in undifferentiated (*UD*) cells, 20 $\mu$g of total protein of SCF was used, and the blots were probed with anti-smac antibody. Shown are representative results of Smac in: *i*, PC12/C cells containing serum (0) deprived of serum for times indicated (h); *ii*, undifferentiated PC12/Bcl-2; and *iii*, PC12/Akt cells deprived of serum. Results of actin are shown as control for loading. The autoradiograms were quantified and % increase in cytosolic Smac was calculated using the intensity value at 0 h as control. The results are expressed as mean ± S.E. ($n$ = 3–4). *, $p < 0.05$ PC12/Bcl-2 and Akt *versus* PC12/C cells. *B*, Smac levels in differentiated PC12 cells (0) deprived of NGF/$Bt_2$cAMP at times indicated (h). Shown are representative results of Smac in SCF in: *i*, PC12/C cells; *ii*, PC12/Bcl-2 cells; and *iii*, PC12/Akt cells. Quantification of autoradiograms are represented as % increase (mean ± S.E., $n$ = 3–4) in Smac in cytosolic fraction. *C*, 30 $\mu$g of total protein of SCF was used for HtrA2/Omi analysis in trophic-deprived undifferentiated (*i*) and differentiated (*ii*) PC12/C for the times indicated.

caspase 9 cascade, is an important determinant of cytochrome *c* sensitivity in undifferentiated and differentiated cells. To ascertain the role of differentiation, we first examined for changes in levels of c-IAP-2 and XIAP as well as Smac/DIABLO andOmi/HtrA2 in undifferentiated *versus* differentiated cells (Fig. 7*A*). Quantification of the results using actin as control in each case showed that the levels of XIAP, Smac/DIABLO, and Omi/HtrA2 remain the same, however there is 41 ± 3% ($n$ = 3) increase in c-IAP-2 levels in differentiated cells. Next we analyzed the levels of XIAP and c-IAP-2 during deprivation of trophic support. In undifferentiated PC12/C, Bcl-2, or Akt cells, XIAP protein levels were unaltered following withdrawal of serum (Fig. 7*B*). In contrast, in PC12/C-differentiated cells, withdrawal of NGF/$Bt_2$cAMP resulted in decreased level of XIAP at 24 h (25–35%) (Fig. 7*C*). This change in XIAP protein level was not seen in differentiated PC12/Akt or PC12/Bcl-2 cells following deprivation of NGF/$Bt_2$cAMP (Fig. 7*C*). In contrast to XIAP, there were no changes in c-IAP-2 levels (data not shown). Taken together with the above AVPI data, these results suggest that XIAP and c-IAP-2 play a role in regulating caspase 9 cascade in differentiated but not undifferentiated cells. To further examine this possibility, we constructed an inducible XIAP-tetracycline-repressible PC12 cell line to examine whether sensitivity to microinjected cytochrome *c* decreases in undifferentiated cells. Undifferentiated PC12 cells in the presence or absence of doxycycline were microinjected with 2, 10, and 25 $\mu$M cytochrome *c*, and cell death was quantified after 6 h (Fig. 7*D*). In sharp contrast to results obtained with PC12/C, PC12/Bcl-2, and PC12/Akt cells (*cf.* Fig. 3, *A* and *B*), these cells were resistant to microinjected cytochrome *c*. However, in the presence of doxycycline these cells were not as sensitive to microinjected cytochrome *c* as PC12/C cells (*cf.* Fig. 3, *A* and *B*). The highest concentration of doxycycline that these cells could tolerate was 0.5 $\mu$g/ml, which may not completely repress tetracycline. The results of immunoblot analysis of XIAP in the absence and presence indicate that XIAP levels are higher in doxycycline-treated cells (Fig. 7*D*). Nevertheless, inhibition of cell death was greater in cells in which doxycycline was withdrawn. Quantification of cell death upon deprivation of trophic support for 24 h in both undifferentiated and differentiated cells showed cell death that is less efficient in the absence than in presence of doxycycline (Fig. 7*E*). In PC12/XIAP cells, cell death in the presence of doxycycline was less compared with PC12/C cells (*cf.* Figs. 1*B* and 2*B*). Overall the results indicate that both XIAP and c-IAP-2 regulate caspase 9 and possibly caspases 7 and 3 activation in differentiated cells.

## DISCUSSION

The characteristics of PC12 cells make them a useful and tractable *in vitro* model with which to examine the parameters regulating cell survival in both proliferating neuroectoderm-derived neoplastic cells and in differentiated neuronal cells. In this study, we have shown that hcC, Smac/DIABLO, and Omi/HtrA2 are released from the mitochondrial compartment of factor-deprived PC12 cells undergoing apoptosis. Moreover, ectopic expression of a dominant interfering mutant of caspase 9 inhibits such cell death. Thus, the mitochondrial hcC-caspase 9-cell death pathway is both activated and important in determining cell death of factor-deprived PC12 cells. We also investigated the regulation exerted by Bcl-2 and activated-Akt on hcC and Smac/DIABLO release from mitochondria and the induction of cell death by cytosolic hcC and caspase 9 activation. We find that in both undifferentiated and differentiated (post-mitotic) PC12 cells, Bcl-2 and Akt exert a suppressive effect on release of hcC and Smac/DIABLO, the effect persisting longer in differentiated cells. Moreover, in contrast to un-

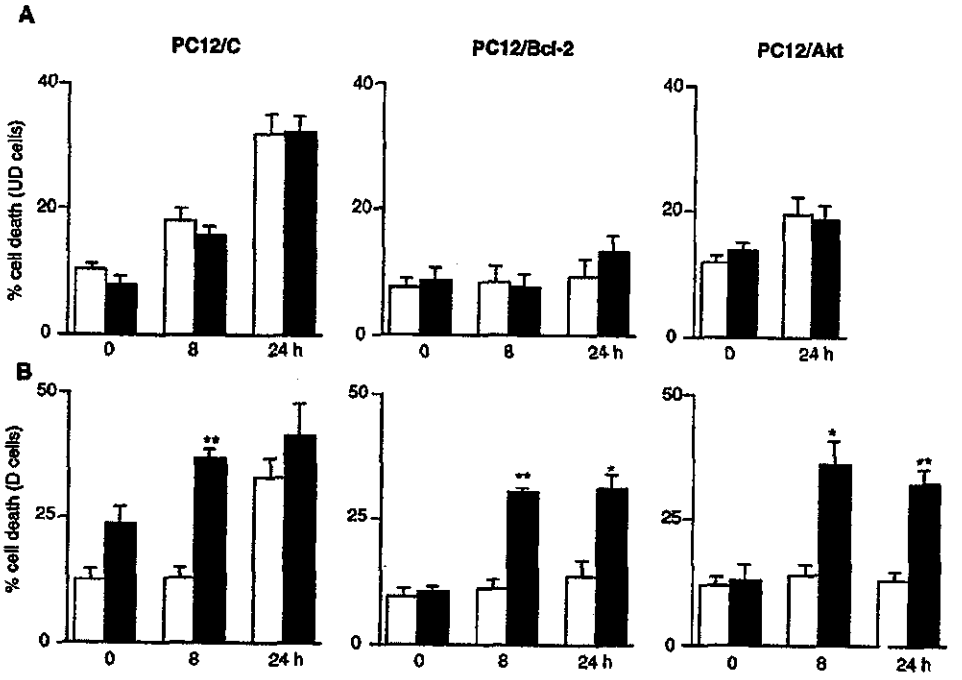


FIG. 6. **Transient co-transfection of PC12 cells with GFP plus Ub-ΔN-AVPI or MVPI Smac/DIABLO.** *A*, undifferentiated PC12/C, PC12/Bcl-2, and PC12/Akt cells were co-transfected with pEGFP and either Ub-ΔN-AVPI (*solid square*) or Ub-ΔN-MVPI (*open square*) Smac/DIABLO. Cell death was quantified in the presence of serum (0 h) and after 8 and 24 h of serum deprivation. The results are mean ± S.E. ($n$ = 3). *B*, results of cell death following co-transfection with Ub-ΔN-AVPI (■) or Ub-ΔN-MVPI (□) Smac/DIABLO in differentiated PC12/C, PC12/Bcl-2, and PC12/Akt containing NGF/$Bt_2$cAMP (0 h) and after withdrawal of NGF/$Bt_2$cAMP for 8 and 24 h. The results are mean ± S.E. ($n$ = 3). *, $p < 0.05$; **, $< 0.01$; in Ub-ΔN-AVPI *versus* Ub-ΔN-MVPI transfected cells (Student's $t$ test, two-tailed).

differentiated cells, in differentiated PC12 cells, Bcl-2 and activated Akt also inhibit the subsequent activation of caspase 9. Further analysis concerning regulation of the caspase 9 pathway by Smac/DIABLO and XIAP indicate that in differentiated but not undifferentiated cells, the IAP binding motif of Smac/DIABLO plays an important role in activating caspase 9 pathway, most likely, by alleviating IAP inhibition. These results strongly suggest that the PC12 differentiation program alters regulation of events downstream of mitochondrial release of apoptogenic factors.

*Release of hcC, Smac/DIABLO, and Omi/HtrA2 from Mitochondria in Factor-deprived PC12 Cells*—In cell death induced by trophic factor deprivation, we observed high cytosolic hcC levels in both undifferentiated and NGF/$Bt_2$cAMP-differentiated PC12 cells. In addition to hcC, the processed forms of both Smac/DIABLO and Omi/HtrA2 were also released from mitochondria during factor-deprivation in PC12 cells. The kinetic analysis revealed an early cytosolic accumulation of these proteins, already evident by 4 h of factor deprivation. However, the peak DEVD cleaving activity occurred at around 16 h (data not shown) just preceding cell death. Because we observed a significant delay before caspases were activated, even though these proteins are released rapidly from mitochondria, this indicates mitochondrial release of these factors is not the rate-limiting event for apoptosis. This result is in accordance with previous findings that, although release of hcC from mitochondria is a critical early event in caspase activation, it does not coincide with the commitment point to cell death (32, 41). Moreover, in response to apoptotic signals such as factor withdrawal, cells can withstand high cytosolic hcC levels and survive as long as caspase activation is inhibited and mitochondrial function maintained (30, 42). Other factors, for example, attainment of optimal cytoplasmic levels of these released proteins, may also play a role in determining the activation of the caspase 9 cascade. In this respect, the kinetic data show that in undifferentiated PC12/Bcl-2 and PC12/Akt cells, the release of hcC is less than in PC12/C cells.

The mature Smac/DIABLO and Omi/HtrA2 proteins have an exposed tetrapeptide IAP-binding motif (IBM) at the N terminus, which by binding to XIAP, c-IAP-1, or c-IAP-2 abrogates IAP inhibition of caspase 9 and the effectors caspases 3 and 7, resulting in positive amplification of caspase loop (34). Co-release of these proteins with hcC in factor-deprived PC12 cells suggests that the inhibitors such as IAPs are removed from caspases allowing them to function in cellular demise. The removal may involve degradation of IAPs as shown in the case of XIAP by Omi/HtrA2 (43). In this regard, we find that XIAP levels decrease in differentiated PC12/C cells deprived of trophic support. Omi/HtrA2 may have other targets. For example, the serine protease inhibitor 4-(2-aminoethyl)benzenesulfonyl fluoride hydrochloride was shown to inhibit cleavage of c-IAP-1 by Omi/HtrA2 (44). 4-(2-Aminoethyl)benzenesulfonyl fluoride hydrochloride has also been reported to inhibit caspase 2 processing and cell death in trophic-deprived PC12 cells (45). It is probable that the released Omi/HtrA2 that we observe activates caspase 2, because caspase 2 is cleaved after serum or NGF/$Bt_2$cAMP withdrawal in undifferentiated and differentiated cells, respectively (data not shown). In differentiated and undifferentiated PC12 cells, the release of mitochondrial hcC, as well as of Smac/DIABLO was suppressed by Bcl-2 or constitutively active Akt. Suppression of Smac/DIABLO release by Bcl-2 and Akt presumably damps down a feed-forward mitochondrial amplification loop ensuring that caspases are not activated. Reinforcing this proposition are the results showing that differentiated PC12/Bcl-2 and PC12/Akt cells are sensitive to Ub-ΔN-AVPI-Smac/DIABLO. We observed that the inhibitory effect of Bcl-2 or Akt on mitochondrial release extended for a longer period in differentiated cells compared with undifferentiated PC12 cells. This observation suggests

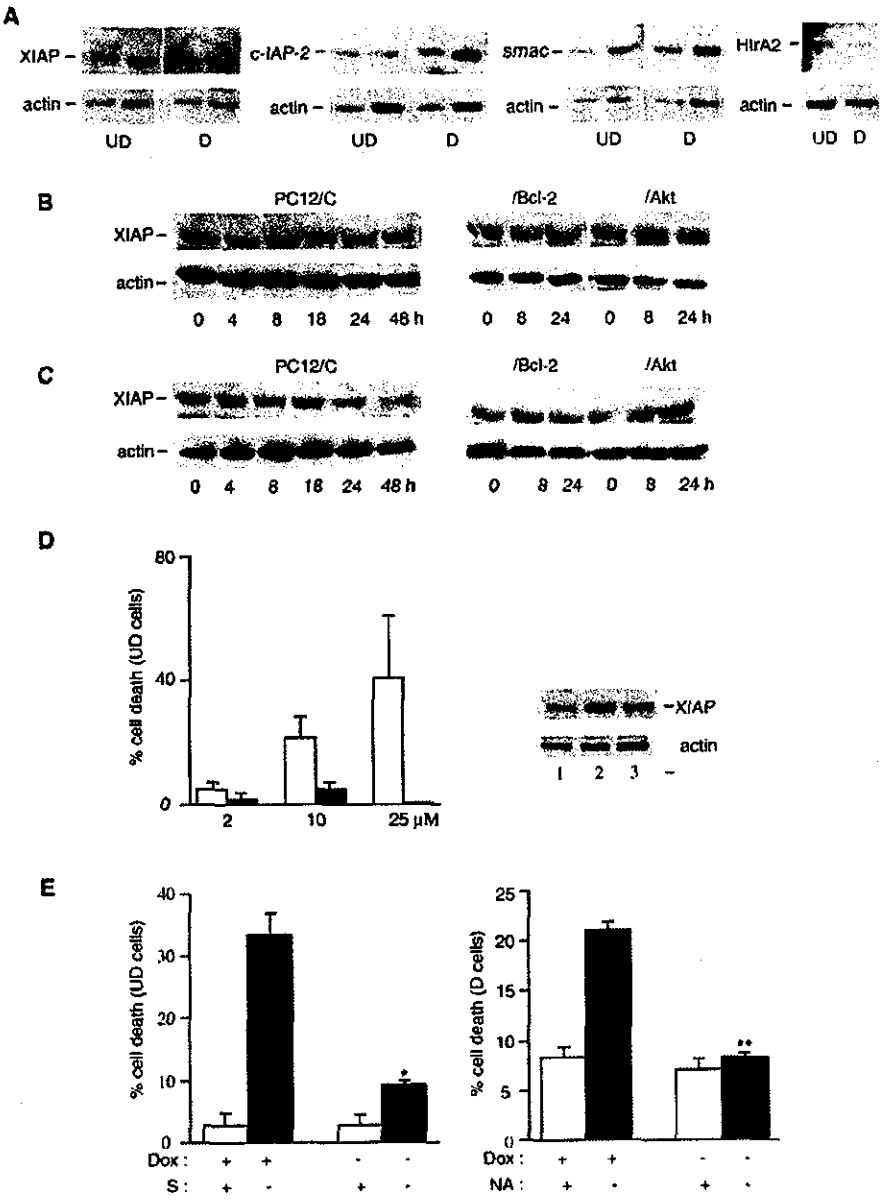


FIG. 7. **Acquisition of IAP regulation of cell death in differentiated cells.** *A*, XIAP, c-IAP-2, Smac, and htrA2 levels were analyzed in undifferentiated (*UD*) and differentiated (*D*) cells using 10 and 20 μg of total protein for XIAP, c-IAP-2, and Smac; and 20 μg for HtrA2. The blots were also analyzed for actin levels. Results were quantified and corrected for protein levels. There is an increase in c-IAP-2 level in differentiated cells. *B*, XIAP levels in undifferentiated PC12/C, PC12/Bcl-2, and PC12/Akt cells following withdrawal of serum. 50 μg of total protein was used, and the same blots were analyzed for actin levels as control for protein loading. *C*, XIAP levels in differentiated PC12/C, PC12/Bcl-2, and PC12/Akt cells containing NGF/$Bt_2$cAMP (0 h) and following withdrawal of NGF/$Bt_2$cAMP at times indicated. *D*, microinjection of cytochrome c in XIAP-tetracycline-repressible undifferentiated PC12/C cells. The cells were co-microinjected with rhodamine and concentrations of cytochrome c as shown, in the presence (*open square*) and in the absence (*solid square*) of doxycycline. Cell death was analyzed 6 h later and quantified. Each experiment was done in duplicate, and the results are expressed as mean ± S.D., $n = 2$–3. *Right panels*: analysis of XIAP protein in PC12/C (*1*) and in PC12/XIAP cells, in the absence (*2*) and presence (*3*) of doxycycline. *E*, cell death following withdrawal of trophic support in XIAP-tetracycline repressible undifferentiated (*UD*) and differentiated (*D*) PC12 cells. Cell death was analyzed in cells containing doxycycline in the presence and absence of serum (*S*) in undifferentiated cells or NGF/$Bt_2$cAMP (*NA*) in differentiated cells. Doxycycline was withdrawn for about 16 h prior to testing cell death in the presence or absence trophic support. The results are expressed as mean ± S.E., $n = 4$. *, $p < 0.05$; **, $p < 0.001$; in the presence of doxycycline *versus* in the absence of doxycycline.

that differentiation has possibly modulated processes, which are involved in translocating these proteins from mitochondria to cytoplasm, and that control at this level is more stringent in differentiated cells.

*Regulation of Cell Death Post-hcC Release from Mitochondria*—Directly introducing cytochrome *c* into PC12 cells by microinjection triggers apoptosis. Such apoptosis must involve activation of caspase 9 for the following reasons: First, the ability of cytoplasmic extracts to induce *in vitro* processing of procaspase 9 mirrored cell death that was observed with microinjected cytochrome *c*. Second, endogenous procaspase 9 was cleaved in trophic factor-deprived cells. Third, cell death was suppressed by expression of a dominant negative caspase 9 mutant. Caspase 9 is activated when holocytochrome c, translocated from mitochondria, induces oligomerization of Apaf-1, a process dependent on ATP (16, 46, 47). Procaspase 9, which is either already associated with Apaf-1 as a holoenzyme (16) or recruited following hcC release, is then cleaved and activated within this "apoptosome complex."

Undifferentiated PC12 cells exhibited markedly greater sensitivity to induction of apoptosis by microinjected cytochrome *c* than differentiated cells. Additionally, NGF, Bcl-2, or constitutively active Akt were ineffective in protecting undifferentiated PC12 cells against microinjected cytochrome *c*. The greater sensitivity cannot simply be explained by differences in surface area (differentiated cells have approximately 1.5× greater surface area) as microinjections of even low concentrations of cytochrome *c* induced cell death that was not inhibited by anti-apoptotic factors. In sharp contrast, resistance to microinjected cytochrome *c* was found in differentiated PC12 cells; there are a delay period before cell death occurred indicating that the differentiation process enables the cells to withstand, for longer periods, the lethal effects of high cytosolic cytochrome *c*. In addition, Bcl-2 and Akt strongly suppressed microinjected cytochrome *c*-induced cell death in differentiated PC12 cells. Bcl-2 was more effective in this regard than Akt; however, their effects may simply be a reflection of levels of expression. The inhibitory effect that we observed in cytosolic extracts from PC12/Bcl2 and PC12/Akt cells correlates with a lack of procaspase 9 processing in response to cytochrome *c* addition. The specific post-mitochondrial action of AVPI-Smac/DIABLO in differentiated cells as well as up-regulation of

c-IAP-2 suggests that the caspase 9 cascade is inhibited by IAPs in differentiated cells but not in undifferentiated cells. In this regard, the induction of chicken IAP protein, ITA, by NGF in sympathetic neurons has been shown to suppress cell death in the absence of NGF (48). The AVPI motif binds to the BIR3 domain of XIAP relieving inhibition of caspase 9, which suggests that XIAP inhibition of caspase 9 is critical for cell death regulation in differentiated PC12 cells. This may explain the greater sensitivity to cytochrome *c* seen in undifferentiated cells. The observation that undifferentiated XIAP-tetracycline-repressible PC12 cells were not very sensitive to microinjected cytochrome *c* strongly indicates that XIAP-mediated inhibition of caspase 9 is acquired during a differentiation program of PC12 cells. A significant resistance to cell death induced by cytochrome *c* microinjection (greater than NGF/$Bt_2$cAMP-differentiated PC12 cells) has been reported in NGF-differentiated and -dependent sympathetic neurons (49). Moreover, it was shown recently that exogenous Smac/DIABLO could relieve this resistance to cytochrome *c* (50) and that deprivation of NGF results in down-regulation of XIAP (51). We have previously shown that cell death induced by deprivation of NGF/$Bt_2$cAMP in differentiated PC12 cells is not dependent on protein synthesis (26, 52), thus it is also likely that there are differences in the regulatory mechanisms of cell death in trophic factor-deprived differentiated PC12 cells and sympathetic neurons.

In conclusion, our PC12 data raise the possibility that during neuronal differentiation additional anti-apoptotic controls are acquired, particularly at the level of procaspase 9 processing and activation. These controls are likely to be important determinants in the long term survival of differentiated post-mitotic neurons.

*Acknowledgments*—We thank all the members of the Evan laboratory for their help and constructive discussions. Our thanks to Dr. Lazebnik for caspase 9 dominant negative plasmid. We are grateful to Drs. T. Littlewood, J. Downward, P. Meier, S. O'Regan, and N. Faucon Biguet for their help with the manuscript, M. Darmon for confocal microscopy, and A. Prochiantz for continued support.

REFERENCES

1. Oppenheim, R. (1991) *Annu. Rev. Neurol.* **14,** 453–501
2. Raff, M. C., Barres, B. A., Burne, J. F., Coles, H. S., Ishizaki, Y., and Jacobson, M. D. (1993) *Science* **262,** 695–700
3. Pettman, B., and Henderson, C. E. (1998) *Neuron* **20,** 633–647
4. Kuida, K., Zheng, T., Na, S., Kuan, C.-Y., Yang, D., Karasuyama, H., Rakic, P., and Flavell, R. (1996) *Nature* **384,** 368–372
5. Kuida, K., Haydar, T. F., Kuan, C.-Y., Gu, Y., Taya, C., Karasuyama, H., Su, M. S., Rakic, P., and Flavell, R. A. (1998) *Cell* **94,** 325–327
6. Motoyama, N., Wang, F., Roth, K., Sawa, H., Nakayama, K.-I., Nakayama, K., Negishi, I., Senju, S., Zhang, Q., Fujii, S., and Loh, D. (1995) *Science* **267,** 1506–1510
7. Yoshida, H., Kong, Y.-Y., Yoshida, R., Elia, A. J., Hakem, A., Hakem, R., Penninger, J. M., and Mak, T. W. (1998) *Cell* **94,** 739–750
8. De La Rosa, E., and de Pablo, F. (2000) *Trends Neurosci.* **23,** 454–458
9. Roth, K. A., Kuan, C.-Y., Hayder, T. F., D'Sa-Eipper, C., Shindler, K. S., Zheng, T. S., Kuida, K., Flavell, R. A., and Rakic, P. (2000) *Proc. Natl. Acad. Sci. U. S. A.* **97,** 466–471
10. Zaidi, A. U., D'Sa-Eipper, C., Brenner, J., Kuida, K., Zheng, T. S., Flavell, R. A., Rakic, P., and Roth, K. A. (2001) *J. Neurosci.* **21,** 169–175
11. Su, J. H., Anderson, A. J., Cummings, B. J., and Cotman, C. W. (1994) *Neuroreport* **5,** 2529–2533
12. Hartmann, A., Hunot, S., Michel, P. P., Muriel, M.-P., Vyas, S., Faucheux, B. A., Mouatt-Prignet, A., Turmel, H., Srinivasan, A., Ruberg, M., Evan, G. I., Agid, Y., and Hirsch, E. C. (2000) *Proc. Natl. Acad. Sci. U. S. A.* **97,** 2875–2880
13. Thornberry, N. A., and Lazebnik, Y. (1998) *Science* **281,** 1312–1316
14. Nicholson, D. W. (1999) *Cell Death Differ.* **6,** 1028–1042
15. Budihardjo, I., Oliver, H., Lutter, M., Luo, X., and Wang, X. (1999) *Annu. Rev. Cell Dev. Biol.* **15,** 269–290
16. Rodriguez, J., and Lazebnik, Y. (1999) *Genes Dev.* **13,** 3179–3184
17. Golstein, J. C., Waterhouse, N. J., Juin, P., Evan, G. I., and Green, D. R. (2000) *Nat. Cell Biol.* **2,** 156–162
18. Green, D. R., and Reed, J. C. (1998) *Science* **281,** 1309–1312
19. Van der Heiden, M. G., and Thompson, C. B. (1999) *Nat. Cell Biol.* **1,** E209–E216
20. Desagher, S., and Martinou, J.-C. (2000) *Trends Cell Biol.* **10,** 369–377
21. Du, C., Fang, M., Li, Y., Li, L. X., and Wang, X. (2000) *Cell* **102,** 33–42
22. Suzuki, Y., Imai, Y., Nakayama, H., Takahashi, K., Takio, K., and Takahashi, R. (2001) *Mol. Cell* **8,** 613–621
23. Martins, L. M., Iaccarino, I., Tenev, T., Gschmeissner, S., Totty, N. F., Lemoine, N. R., Savopoulos, J., Gray, C. W., Creasy, C. L., Dingwall, C., and Downward, J. (2002) *J. Biol. Chem.* **277,** 439–444
24. Datta, S. R., Brunet, A., and Greenberg, M. E. (1999) *Genes Dev.* **13,** 2905–2927
25. Kennedy, S. G., Kandel, E. S., Cross, T. K., and Hay, N. (1999) *Mol. Cell. Biol.* **19,** 5800–5810
26. Michel, P. P., Vyas, S., and Agid, Y. (1995) *Eur. J. Neurosci.* **7,** 577–586
27. Yao, R., and Cooper, G. M. (1995) *Science* **267,** 2003–2006
28. Troy, C. M., Stefanis, L., Greene, L. A., and Shelanski, M. L. (1997) *J. Neurosci.* **17,** 1911–1918
29. Troy, C. M., Rabacchi, S. A., Hohl, J. B., Angelastro, J. M., Greene, L. A., and Shelanski, M. L. (2001) *J. Neurosci.* **21,** 5007–5016
30. Deshmukh, M., Kuida, K., and Johnson, E. M., Jr. (2000) *J. Cell Biol.* **150,** 131–143
31. Srinivasula, S. M., Ahmad, M., Fernandes-Alnemri, T., and Alnemri, E. S. (1998) *Mol. Cell* **1,** 949–957
32. Juin, P., Hueber, A.-O., Littlewood, T., and Evan, G. I. (1999) *Genes Dev.* **13,** 1367–1381
33. Kluck, R. M., Bossy-Wetzel, E., Green, D. R., and Newmeyer, D. D. (1997) *Science* **275,** 1132–1136
34. Shi, Y. (2002) *Mol. Cell* **9,** 459–470
35. Fearnhead, H. O., Rodriguez, J., Govek, E.-E., Guo, W., Kobayashi, R., Hannon, G., and Lazebnik, Y. A. (1998) *Proc. Natl. Acad. Sci. U. S. A.* **95,** 13664–13669
36. Goyal, L. (2001) *Cell* **104,** 805–808
37. Liu, Z., Sun, C., Olejniczak, E. T., Meadows, R. P., Betz, S. F., Oost, T., Herrmann, J., Wu, J. C., and Fesik, S. W. (2000) *Nature* **408,** 1004–1008
38. Wu, G., Chai, J., Suber, T. L., Wu, J.-W., Du, C., Wang, X., and Shi, Y. (2000) *Nature* **408,** 1008–1012
39. Hunter, A. M., Kottachchi, D., Lewis, J., Duckett, C. S., Korneluk, R. G., and Liston, P. (2003) *J. Biol. Chem.* **278,** 7494–7499
40. Roberts, D. L., Merrison, W., MacFarlane, M., and Cohen, G. M. (2001) *J. Cell Biol.* **153,** 221–227
41. Kroemer, G., and Reed, J. C. (2000) *Nat. Med.* **6,** 513–519
42. Martinou, I., Desagher, S., Eskes, R., Antonsson, B., Andre, E., Fakan, S., and Martinou, J.-C. (1999) *J. Cell Biol.* **144,** 883–889
43. Srinivasula, S. M., Gupta, S., Datta, P., Zhang, Z., Hedge, R., Cheong, N., Fernandes-Alnemri, T., and Alnemri, E. S. (2003) *J. Biol. Chem.* **278,** 31469–31472
44. Jin, S., Kalkum, M., Overholtzer, M., Stoffel, A., Chait, B. T., and Levine, A. J. (2003) *Genes Dev.* **17,** 1–9
45. Stefanis, L., Troy, C. M., Qi, H., and Greene, L. A. (1997) *J. Neurochem.* **69,** 1425–1437
46. Li, P., Nijhawan, D., Budihardjo, I., Srinivsula, S., Ahmad, M., Alnemeri, E., and Wang, X. (1997) *Cell* **91,** 479–489
47. Saleh, A., Srinivasula, S. M., Acharya, S., Fishel, R., and Alnemri, E. S. (1999) *J. Biol. Chem.* **274,** 17941–17945
48. Wiese, S., Digby, M., Gunnersen, J., Gotz, R., Pei, G., Holtmann, B., Lowenthal, J., and Sendtner, M. (1999) *Nat. Neurosci.* **2,** 978–983
49. Deshmukh, M., and Johnson, E. M., Jr. (1998) *Neuron* **21,** 695–705
50. Deshmukh, M., Du, C., Wang, X., and Johnson, E. M., Jr. (2002) *J. Neurosci.* **22,** 8018–8027
51. Potts, P. R., Singh, S., Knezek, M., Thompson, C. B., and Deshmukh, M. (2003) *J. Cell Biol.* **163,** 789–799
52. Vyas, S., Biguet, N. F., Michel, P. P., Monaco, L., Foulkes, N. S., Evan, G. I., Sassone-Corsi, P., and Agid, Y. (2002) *Mol. Cell Neurosci.* **21,** 1–14

*Human Molecular Genetics, 2004, Vol. 13, No. 19* **2183–2196**
*doi:10.1093/hmg/ddh246*
*Advance Access published on August 4, 2004*

# Calcium-permeable AMPA receptors promote misfolding of mutant SOD1 protein and development of amyotrophic lateral sclerosis in a transgenic mouse model

**Minako Tateno[1], Hisako Sadakata[1], Mika Tanaka[2], Shigeyoshi Itohara[2], Ryong-Moon Shin[3], Masami Miura[3], Masao Masuda[3], Toshihiko Aosaki[3], Makoto Urushitani[1], Hidemi Misawa[4] and Ryosuke Takahashi[1,*]**

[1]Laboratory for Motor System Neurodegeneration and [2]Laboratory for Behavioral Genetics, Brain Science Institute, RIKEN, Wako, Saitama 351-0198, Japan, [3]Neural Circuits Dynamics Research Group, Tokyo Metropolitan Institute of Gerontology, Itabashi, Tokyo 173-0015, Japan and [4]Department of Neurology, Tokyo Metropolitan Institute for Neuroscience, Fuchu, Tokyo 183-8526, Japan

Received April 21, 2004; Revised and Accepted July 20, 2004

**Mutant Cu/Zn-superoxide dismutase (SOD1) protein aggregation has been suggested as responsible for amyotrophic lateral sclerosis (ALS), although the operative mediating factors are as yet unestablished. To evaluate the contribution of motoneuronal $Ca^{2+}$-permeable (GluR2 subunit-lacking) α-amino-3-hydroxy-5-methyl-4-isoxazole propionic acid (AMPA)-type glutamate receptors to SOD1-related motoneuronal death, we generated *chat-GluR2* transgenic mice with significantly reduced $Ca^{2+}$-permeability of these receptors in spinal motoneurons. Crossbreeding of the *hSOD1*$^{G93A}$ transgenic mouse model of ALS with *chat-GluR2* mice led to marked delay of disease onset (19.5%), mortality (14.3%) and the pathological hallmarks such as release of cytochrome *c* from mitochondria, induction of *cox2* and astrogliosis. Subcellular fractionation analysis revealed that unusual SOD1 species first accumulated in two fractions dense with neurofilaments/glial fibrillary acidic protein/nuclei and mitochondria long time before disease onset, and then concentrated into the former fraction by disease onset. All these processes for unusual SOD1 accumulation were considerably delayed by GluR2 overexpression. $Ca^{2+}$-influx through atypical motoneuronal AMPA receptors thus promotes a misfolding of mutant SOD1 protein and eventual death of these neurons.**

## INTRODUCTION

Amyotrophic lateral sclerosis (ALS) is a fatal, adult-onset neurodegenerative disease characterized by a selective loss of motoneurons in the spinal cord and brainstem (1). Mutation of Cu/Zn-superoxide dismutase (SOD1) is the most frequent cause of familial ALS (2). Introduction of such mutated SOD1 genes into mice causes ALS-like symptoms characterized by the selective death of spinal motoneurons, despite a ubiquitous expression of mutant proteins (3). Several lines of evidence have demonstrated that mutant SOD1 toxicity is not essentially due to decreased dismutase activity, but rather to a 'gain of toxic function' (4). This so-called 'oligomerization hypothesis' has recently attracted attention from ALS researchers. The hypothesis maintains that mutant SOD1 proteins are misfolded, and consequently oligomerized and aggregated, gaining toxic properties at some stage in their formation (5). The hypothesis is based on the numerous observations that SOD1-containing inclusions/high-molecular-weight-shifted protein complexes are specifically found in spinal motoneurons and their surrounding astrocytes from autopsied patients and transgenic mice carrying mutant SOD1 genes (6–8), in spinal cord extracts from mutant SOD1 transgenic mice (9–12) and in cultured motoneurons into which mutant SOD1 has been microinjected (13).

*To whom correspondence should be addressed at: Laboratory for Motor System Neurodegeneration, Brain Science Institute, Riken, 2-1 Hirosawa, Wako, Saitama 351-0198, Japan. Tel: +81 484676072; Fax: +81 484624796; Email: ryosuke@brain.riken.jp

However, in addition to this line of evidence, glutamate-induced excitotoxicity has also been implicated in the pathophysiology of ALS patients and mutant SOD1 transgenic mice (14–17). Pharmacological experiments have strongly suggested that the excitotoxicity of spinal motoneurons largely depends on $Ca^{2+}$-permeable α-amino-3-hydroxy-5-methyl-4-isoxazole propionic acid (AMPA) receptors specifically expressed in a subset of neurons, including spinal motoneurons (18,19). AMPA receptors, major mediators for fast excitatory neurotransmission in the mammalian central nervous system, are composed of a heteromeric complex of four subunits GluR1–GluR4, and the absence of GluR2 renders the receptor $Ca^{2+}$-permeable (20). As this unique property of GluR2 is generated posttranscriptionally by RNA editing, an editing failure can also produce $Ca^{2+}$-permeable AMPA receptors (21). Reduced editing efficiency of GluR2 mRNA has been specifically reported in spinal motoneurons from human sporadic ALS patients (22), further suggesting that $Ca^{2+}$-permeable AMPA receptor-mediated excitotoxicity is closely linked to the vulnerability of spinal motoneurons in ALS. However, whether and in what manner this atypical type of AMPA receptor affects mutant SOD1-induced motoneuronal degeneration remains to be elucidated.

The purpose of the present study was to explore a mechanistic link between glutamate toxicity and the conversion of mutant SOD1 into aberrant forms by modification of the electrophysiological properties of motoneuronal AMPA receptors in an ALS mouse model. The *chat-GluR2* transgenic mouse line was generated to overexpress *GluR2* in a cholinergic neuron-specific manner, resulting in a large reduction in $Ca^{2+}$-permeability of motoneuronal AMPA receptors. We detected various types of abnormally folded SOD1 proteins in fractions derived from different cellular compartments from *hSOD1*$^{G93A}$ mice spinal cords. Double transgenic mice carrying both *chat-GluR2* and *hSOD1*$^{G93A}$ displayed a marked delay of disease onset, followed by delayed formation of all the abnormal SOD1 species. These results indicate that $Ca^{2+}$-permeable AMPA receptors in motoneurons contribute to the conformational changes of mutant SOD1 and the subsequent neurodegeneration associated with these changes.

## RESULTS

### Generation and characterization of *chat-GluR2* transgenic mice: cholinergic neuron-specific GluR2 overexpression results in substantial reduction of $Ca^{2+}$-permeable AMPA receptors in spinal motoneurons

A mouse line with reduced numbers of $Ca^{2+}$-permeable AMPA receptors in spinal motoneurons was generated. Spinal motoneurons are typical cholinergic neurons, constituting a minor population among total spinal neurons. Thus, a cholinergic neuron-specific promoter, i.e. the choline acetyltransferase (*ChAT*) gene promoter (23) (Fig. 1A) was used to preferentially increase *GluR2* expression in spinal motoneurons. Three independent *chat-GluR2* transgenic lines, Tg3, Tg7 and Tg10, were established. To examine the copy number of the *chat-GluR2* transgene, Taqman quantitative DNA PCR and genomic Southern blotting were performed. Results from Taqman PCR indicated that the Tg3, Tg7 and Tg10 lines contained ~2, 10 and 16 copies of the *chat-GluR2* transgene, respectively, a finding which was also supported by genomic Southern blotting (Fig. 1B). Expression patterns of the transgenes in the spinal cord were examined using *in situ* hybridization (Fig. 1C), revealing a preferential transcription of transgenes in cholinergic neurons in *chat-GluR2* mice. To quantify the *GluR2* mRNA level in spinal motoneurons, motoneurons were carefully purified from frozen slices of spinal cord using laser microdissection, because other neuronal populations such as dorsal horn neurons express high level of *GluR2*. Quantitative PCR analysis revealed that spinal motoneurons in Tg7 expressed levels of *GluR2* mRNA nearly 5-fold higher than those of non-transgenic control mice (Table 1). Tg10 included numerous copies of the transgene, but displayed lower levels of *GluR2* expression than Tg7, probably owing to DNA methylation of transgenes (data not shown). No significant changes in mRNA levels of *ChAT*, endogenous *SOD1*, *GluR3* or *GluR4* were observed in *chat-GluR2* transgenic mice compared with non-transgenic mice. Western blotting of the extracts prepared from the spinal cord ventral region also revealed a significant increase of the GluR2 protein level in Tg7 compared with that in non-transgenic littermates (Fig. 1D). *GluR2* expression was thus significantly increased in spinal motoneurons in *chat-GluR2* mice without affecting the expression of other AMPA receptor subunits. Next, the $Ca^{2+}$-permeability of AMPA receptors in spinal motoneurons was examined. Whole-cell patch-clamp recordings were performed on motoneurons in spinal cord slices. The first two graphs in Figure 1E represent typical I-V relationships, showing distinct inward rectification in wild-type (wt), whereas a linear relationship is seen in Tg7. Normalized I–V relationships reveal a clear difference between wt and Tg7 ($P < 0.001$). The rectification index, an index of $Ca^{2+}$-permeability calculated as the ratio of chord conductance at +40 and −70 mV, was estimated as $0.262 \pm 0.024$ for wt and $0.436 \pm 0.038$ for Tg7 (mean ± SEM, $P < 0.001$). Thus, the majority of AMPA receptors in spinal motoneurons were $Ca^{2+}$-impermeable in Tg7 mice, but were $Ca^{2+}$-permeable in non-transgenic controls.

### Crossbreeding *hSOD1*$^{G93A}$ transgenic mice with *chat-GluR2* transgenic mice markedly delays disease onset and mortality

The *chat-GluR2* transgenic mouse was mated with a *hSOD1*$^{G93A}$ transgenic ALS mouse to generate double transgenic (GS) mice. Most of the spinal motoneuronal AMPA receptors were actually $Ca^{2+}$-impermeable in GS mice, but $Ca^{2+}$-permeable in littermates carrying only the *hSOD1*$^{G93A}$ transgene (*S* mice, Fig. 2A). The G1L line of *hSOD1*$^{G93A}$ mice develops overt symptoms defined as disease onset at around 7 months, a classification based on a sudden decrease in motor performance in behavioral tests such as the rotarod test (25,26). Death occurs at around 8.5–9 months. To evaluate the effects of reduced $Ca^{2+}$-permeability in AMPA receptors on the clinical course of ALS, motor performance was assessed by the rotarod test. Figure 2B depicts the rotarod score of each mouse measured every week, clearly showing that mice carrying the *SOD1*$^{G93A}$ gene are rapidly declining

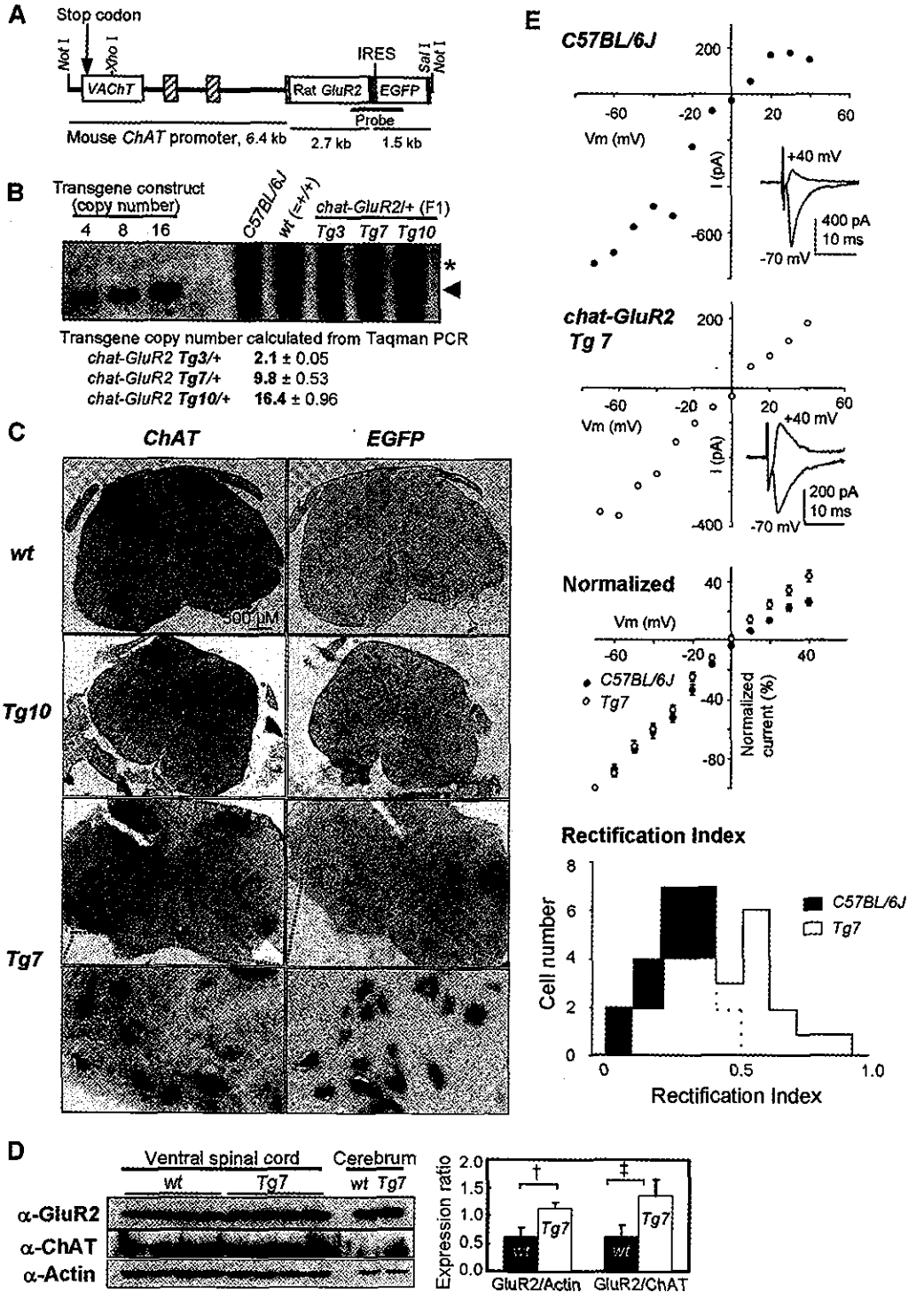


**Figure 1.** Generation and characterization of *chat-GluR2* transgenic mice. (**A**) The DNA fragment introduced into *chat-GluR2* transgenic mice contains the rat *GluR2* and *EGFP* coding sequences driven by mouse *ChAT* promoter. *GluR2* and *EGFP* are transcribed into the same mRNA, but are independently translated owing to the IRES. The striped and filled boxes represent exons of the endogenous *ChAT* gene and SV40 polyadenylation signal, respectively. (**B**) Transgene copy number was examined by genomic Southern blotting using the probe indicated in (A) (24) and by Taqman quantitative DNA PCR. The arrowhead indicates the *Xho*1–*Sal*1-digested 9.0 kb fragment of the transgene. (**C**) Transgene expression is predominant in cholinergic neurons. Either digoxigenin-labeled *EGFP* or *ChAT* riboprobe was used to hybridize to spinal cord sections. Both *EGFP* and *ChAT* were preferentially expressed in large cells (diameter $\geq$25 μm) located in the ventral horn, representing spinal motoneurons. (**D**) The GluR2 protein level is increased in the ventral half of the spinal cord in *chat-GluR2* transgenic mice. The ventral half was carefully dissected from T10–L5 segments of spinal cords. Extracts of ventral spinal cords (40 μg, $n = 4$) and cerebrum (10 μg, $n = 2$) were immunoblotted. † $P < 0.05$, ‡ $P < 0.01$. (**E**) The majority of AMPA receptors in spinal motoneurons were $Ca^{2+}$-impermeable in *chat-GluR2* transgenic mice. The excitatory postsynaptic potential (EPSC) of AMPA components was measured from 23 motoneurons of *chat-GluR2* transgenic mice (Tg7, $n = 11$) and 22 motoneurons of non-transgenic C57BL/6J mice (wt, $n = 9$), using the whole-cell patch-clamp method. Insets represent synaptic currents at holding potentials of −70 and +40 mV.

**Table 1.** GluR2 mRNA level is to increased in motoneurons of *chat-GluR2* transgenic mice

| Mouse | GluR2 | GluR3 | GluR4 | ChAT | SOD1 |
|---|---|---|---|---|---|
| C57BL/6J ($n = 3$) | 1.00 | 1.00 | 1.00 | 1.00 | 1.00 |
| GluR2-Tg3 ($n = 3$) | 0.96 ± 0.27 | 0.91 ± 0.13 | 1.23 ± 0.27 | 1.01 ± 0.16 | 0.74 ± 0.20 |
| GluR2-Tg7 ($n = 3$) | 4.78 ± 0.85* | 1.02 ± 0.54 | 1.21 ± 0.26 | 1.17 ± 0.38 | 1.09 ± 0.41 |
| GluR2-Tg10 ($n = 6$) | 1.58 ± 0.38** | 0.92 ± 0.92 | 1.22 ± 0.48 | 1.15 ± 0.58 | 1.02 ± 0.15 |

Motoneurons in spinal cord were collected using laser microdissection. Transcription levels of several genes were examined by Taqman real-time quantitative PCR. Data were normalized with *GAPDH* expression and then represent relative expression levels compared with levels in C57BL/6J non-transgenic control mice (mean ± SD). Not significantly different ($P > 0.05$) except for *($P = 0.0015$) and **($P = 0.0184$), compared with non-transgenic controls.

in performance score after a certain period. The day just before the decline in score was defined as the day of disease onset, and the mean time of disease onset was compared between S and GS littermates. Disease onset in GS mice was delayed, by 42.9 days (19.5%) in Tg7 and 18.7 days (8.5%) in Tg10, as compared with S mice. Lifespan was also prolonged in GS mice, by 37.5 days (14.3%) in Tg7 and 15.2 days (5.7%) in Tg10 (Fig. 2C, Table 2). No significant difference in rotarod score or lifespan was observed between the *chat-GluR2* and wt mice (data not shown). Furthermore, no prolongation of lifespan was observed in the GS mice generated from Tg3 (data not shown), which animals displayed no additional *GluR2* expression in spinal motoneurons (Table 1). The number of motoneurons in the spinal cord was counted, revealing that degeneration of motoneurons was also delayed in GS mice from the Tg7 line (Fig. 2D). All these results indicate that reducing $Ca^{2+}$-permeability in AMPA receptors delays disease onset and motoneuron death caused by mutant SOD1, presumably in a dose-dependent manner.

### cytochrome *c*-release from mitochondria, *cox2*-induction and gliosis are delayed by GluR2 overexpression

We next investigated whether pathological changes related to disease onset are verifiably affected by overexpression of GluR2. Of the numerous events accompanying disease onset in *hSOD1*$^{G93A}$ mice, we focused on cytochrome *c*-release from mitochondria and induction of cyclooxygenase-2 (*cox-2*), as a treatment of *hSOD1*$^{G93A}$ mice with agents inhibiting these events delays disease onset (26,27). Cytochrome *c*, which is normally localized to the intermembrane space of mitochondria, activates caspases and subsequent apoptosis after release into the cytosol (28). Cox-2 catalyzes the synthesis of prostaglandin E2, which stimulates glutamate release from astrocytes and plays a key role in the inflammatory process (29). Cytosolic extracts (26) and RNA were prepared from the spinal cord lumbar region, as this is the most severely affected region in ALS. Cytochrome *c* became clearly detectable in the cytosolic fraction around 7 months in S, but was only faintly detectable even at 8 months in GS littermates, indicating that the release of cytochrome *c* is considerably delayed in *GS* mice (Fig. 3A). Induction of *cox-2* transcription was also significantly delayed in GS in comparison to S littermates (Fig. 3B). After disease onset, *hSOD1*$^{G93A}$ mice exhibit severe gliosis in the spinal cord owing to exacerbated inflammation (30). We also found that astrogliosis was remarkably delayed in GS mice (Fig. 3C). Reducing $Ca^{2+}$-permeability of AMPA receptors is thus likely to affect the upstream events of cytochrome *c*-release and *cox-2* induction among the processes triggered by mutant *SOD1* proteins.

### Mutant SOD1 protein is converted into various unusual forms in different cellular compartments, but the conversion is markedly delayed by GluR2 overexpression

The misfolding and subsequent conformational changes in mutant SOD1 proteins are hypothesized to be responsible for the death of motoneurons in SOD1-related ALS (5,9,10). Most SOD1 proteins are located in the cytosol, but very small populations are found in organelles such as mitochondria (31) and nuclei (32). Therefore, we roughly divided a homogenate from the lumbar spinal cord into a crude mitochondrial fraction and a post-mitochondrial fraction by simple centrifugation (31), and analyzed in which fraction the misfolded and hence high-molecular-weight-shifted SOD1 proteins were detectable. Most organelles and cytoskeletons were found to be contained in the crude mitochondrial fraction, whereas cytosolic proteins were in the post-mitochondrial fraction (data not shown).

As the post-mitochondrial fraction contained an extremely large amount of SOD1 proteins, it was a formidable task to detect high-molecular-weight-shifted SOD1 species in this fraction by conventional western blotting (data not shown). To enhance the sensitivity of detection, the post-mitochondrial fraction was size-fractionated using size-exclusive chromatography with high-performance liquid chromatography (HPLC), and the HPLC fractions were immunoblotted. The results as shown in Figure 4A indicated that, in addition to the very large amount of SOD1 monomers, high-molecular-weight-shifted SOD1-immunopositive species corresponding to dimer (*2), trimer (*3) and tetramer (*4) sizes of mutant SOD1 were detectable in 2-, 6- and 8-month-old S mice, respectively (Fig. 4A). These oligomer-sized species were not observably detected in the lumbar spinal cord from wt or the cerebrum from S littermates even at 8 months, suggesting that the conversion of the SOD1 protein into oligomer-sized forms preferentially occurs in the spinal cord. The molecular shifts of those species were not due to ubiquitination, as they were not detected by anti-ubiquitin antibody (Supplementary Material, Fig. S1). Formation of oligomer-sized SOD1 aberrant forms

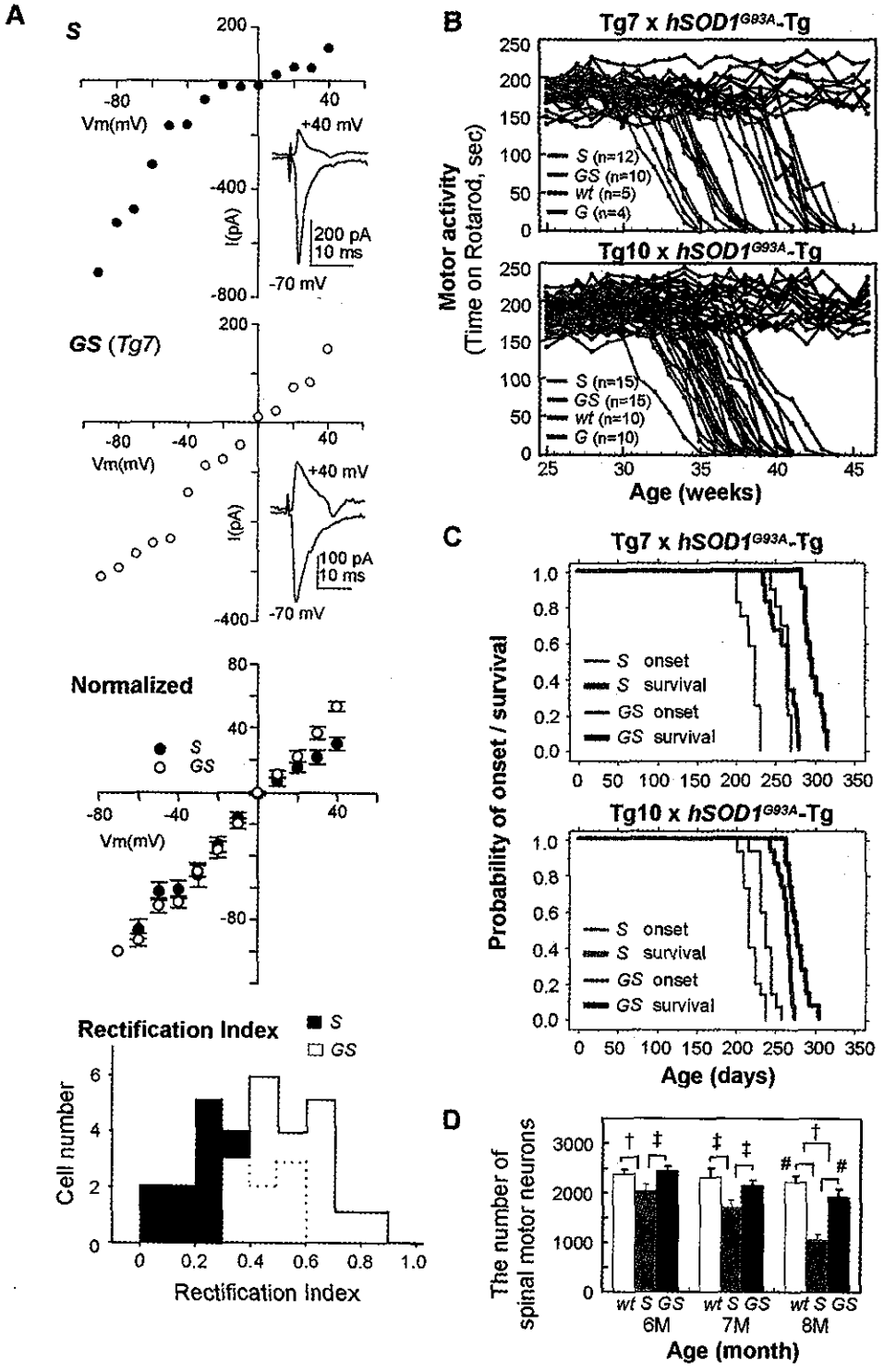


**Figure 2.** GluR2 overexpression markedly delays disease onset and prolongs survival in *hSOD1*$^{G93A}$ transgenic mice. (**A**) The majority of AMPA receptors in spinal motoneurons were $Ca^{2+}$-impermeable in GS (*chat-GluR2/+;hSOD1*$^{G93A}$/+) littermates, but $Ca^{2+}$-permeable in S (*hSOD1*$^{G93A}$/+) littermates. EPSCs of AMPA components were measured from 19 (S, $n = 5$) and 21 (GS, $n = 4$) spinal motoneurons in the same way as in Figure 1E. Rectification index was estimated as 0.321 ± 0.036 for S and 0.535 ± 0.018 for GS (mean ± SEM, $P < 0.01$). (**B**) GluR2 overexpression delayed the decline of motor performance assessed by the rotarod test. Each point represents the mean of four measurements per day every week on each mouse. Significance of difference in comparison of GS versus S littermates was analyzed by repeated measured ANOVA followed by Fisher's PLSD *post hoc* test (Tg7: $P < 0.0001$ and Tg10: $P = 0.0005$). In both lines, $P < 0.001$ after 32 weeks of age. (**C**) Cumulative probability of disease onset and survival was compared between S and GS littermates. Data were analyzed by Kaplan-Meier life test and log-rank test, and the result is summarized in Table 2. (**D**) Degeneration of spinal motoneurons was significantly delayed by GluR2 overexpression. The 30 μm thick frozen sections were prepared from T10–L5 segments of spinal cords and stained with 0.01% toluidine blue. Large neurons with diameter >25 μm in the ventral horn, which are most severely depleted in *hSOD1*$^{G93A}$ mice, were counted serially in all sections. Data represent the means ± SEM from 4–6 mice in each stage. † $P < 0.05$, ‡ $P < 0.01$ and # $P < 0.001$.

**Table 2.** Prolonging effects of *GluR2* overexpression on the disease onset and survival

| *chat-GluR2*-Tg | | *hSOD1*$^{G93A}$/+ | *chat-GluR2*/+, *hSOD1*$^{G93A}$/+ | *P* |
|---|---|---|---|---|
| Tg7 | Onset | 219.7 ± 3.0 | 262.6 ± 2.6 | <0.0001 |
| | Survival | 262.5 ± 4.5 | 300.0 ± 3.5 | <0.0001 |
| | Length | 42.8 ± 2.2 | 37.9 ± 2.4 | 0.1563 |
| | *n* | 12 | 10 | |
| Tg10 | Onset | 219.8 ± 2.6 | 238.5 ± 2.7 | <0.0001 |
| | Survival | 264.5 ± 2.2 | 279.7 ± 3.1 | 0.0005 |
| | Length | 44.8 ± 2.0 | 40.8 ± 2.0 | 0.2189 |
| | *n* | 15 | 15 | |

Data are expressed as means ± SEM. Statistical significance in comparison of *hSOD1*/+ (S) and *chat-GluR2*/+ *hSOD1*/+ (GS) littermates was assessed by ANOVA followed by *post hoc* Fisher's PLSD test.

was significantly delayed in GS compared with S littermates. On the other hand, western blotting of the crude mitochondrial fractions revealed that a significant population of SOD1 proteins in this fraction was converted into species distinct from those found in the post-mitochondrial fractions (Fig. 4B). In addition to dimer-sized SOD1, two major species between the monomer and dimer sizes (~25 and 35 kDa) were detected in symptomatic mice. Formation of all the unusual species in crude mitochondrial fractions was also delayed by more than 1 month in GS compared with S littermates.

Certain populations of SOD1 proteins, probably growing aggregates, can be efficiently trapped onto membranes composed of cellulose acetate, and these filter-trapped SOD1 species extensively increased in tandem with disease progression in mutant SOD1 transgenic mice (10). Figure 4C indicates that the filter-trapped SOD1 aggregates were considerably increased during disease onset in S mice, but increased more slowly in GS compared with S littermates.

### Unusual SOD1 species first accumulate in the fractions dense with neurofilaments, GFAP, nuclei and mitochondria, which accumulation is markedly delayed by GluR2 overxpression

The finding of unusual SOD1 species depicted in Figure 4 led us to do further subcellular fractionation analysis in order to define in which cellular component such unusual species are localized. We thus divided the lumbar spinal cord into four different organelle-enriched fractions (P1–P4) and a supernatant fraction (S) consisting of cytosolic proteins (Fig. 5A). Immunoblots of these fractions revealed that unusual SOD1 species (*) first appeared in the P1 and P2 fractions long time before disease onset, and then, intensively accumulated into the P1 fraction by the disease onset (Fig. 5B). Nuclei and certain kinds of cytoskeletons such as neurofilaments and glial fibrillary acidic protein (GFAP) were effectively concentrated into the P1 fraction, whereas mitochondria are concentrated into the P2 fraction. In S mice, the dimer-sized species were first detected in the P1 and P2 fractions at 4 months. At 7 months, the stage of disease onset, the P1 fraction contained a considerable amount of unusual SOD1 species of approximately the size of a dimer, 25 and 35 kDa, which were very similar to those detected in the crude mitochondrial fractions as depicted in Figure 4B. These species were only weakly detected in P2, P3 and P4 fractions at the stage of disease onset, but then accumulated with disease progression. All these unusual SOD1 species were hardly detectable in the cerebrum, cerebellum, testis and muscle from S mice even at end stage (data not shown for cerebellum and muscle), and were hardly detectable in the spinal cord from 9-month-old wt littermates. In GS littermates, dimer-sized species were faintly detected in the P1 and P2 fractions at 6 months of age. Other species accumulated to an enormous extent in the P1 fraction at 8 months of age, the stage of disease onset in GS mice, indicating that the formation of these unusual SOD1 species was delayed concomitantly with the delay of disease onset in GS compared with S littermates. These observations strongly suggest that the misfolding and subsequent conformational changes of mutant SOD1 proteins are delayed when the $Ca^{2+}$-permeability of AMPA receptors is significantly reduced.

### The increase of oxidatively modified proteins is attenuated by GluR2 overexpression

Although the mechanism underlying the marked effects of reduced AMPA receptor $Ca^{2+}$-permeability on the conformational changes of mutant SOD1 is currently unclear, the attenuation of cellular oxidative stress may be involved. Oxidation of human SOD1 proteins *in vitro* causes cleavage and/or conjugation (33), resulting in the formation of various types of unusual SOD1 species (34,35). Moreover, elevated cellular oxidative stress and resulting oxidative modification of proteins and lipids such as carbonylation are reported in spinal cords from *hSOD1*$^{G93A}$ mice (36–38). Thus, we compared the level of carbonylated proteins in spinal cord extracts between S and GS littermates, taking it as a marker of cellular oxidative stress. The results in Figure 6 reveal that carbonylated proteins in spinal cords increased only gradually before disease onset, then, increased substantially at disease onset in both S and GS mice. Such drastic increase was not observed in the extracts from cerebrum even in 9-month-old S mice. Statistical analysis revealed that the increase of carbonylation was significantly delayed, by at least 2 months, in GS compared with S littermates. This delay of protein oxidative modification might help explain why conformational changes of SOD1 proteins are delayed in GS mice.

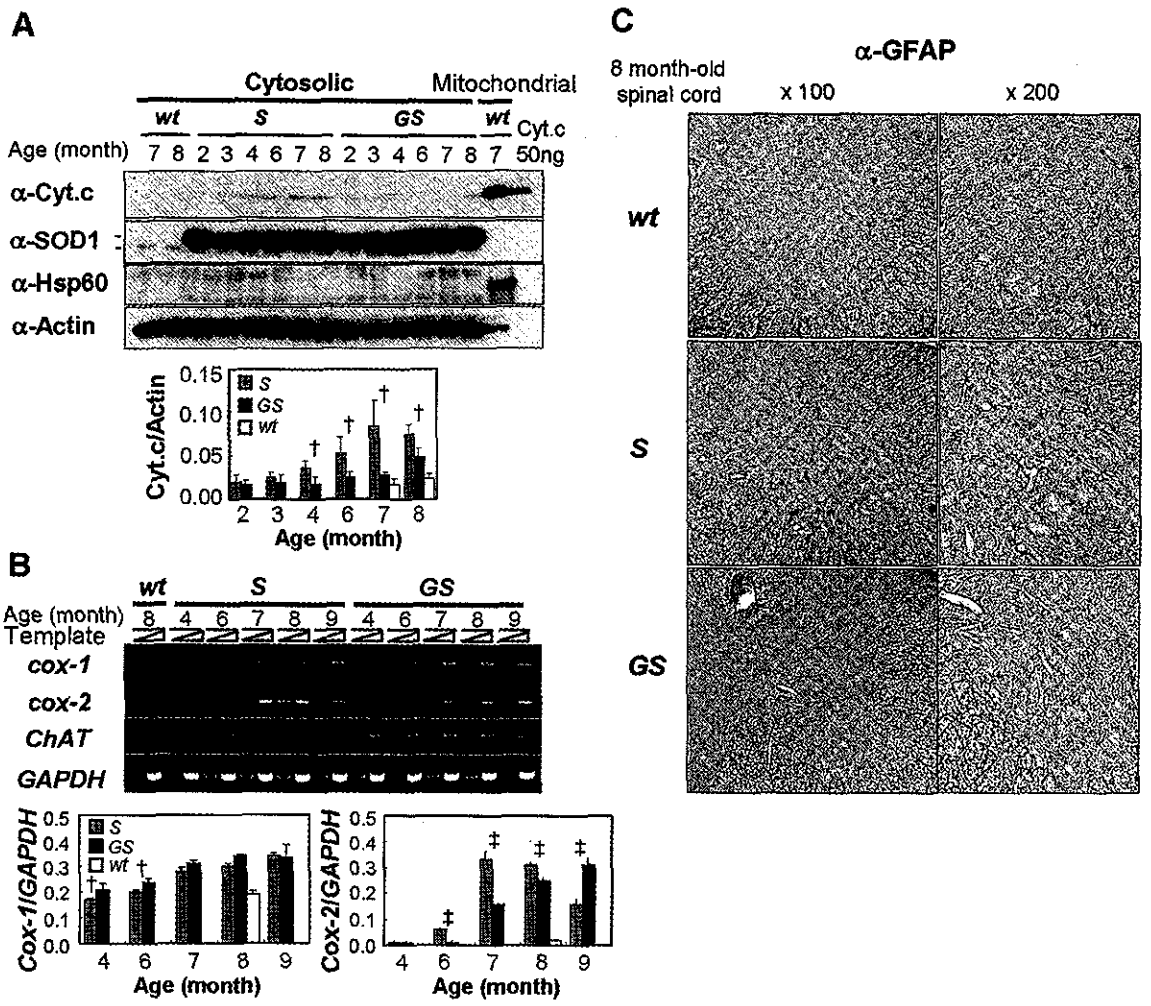


**Figure 3.** GluR2 overexpression delays cytochrome *c*-release from mitochondria, *cox-2* induction and subsequent astrogliosis. (**A**) Cytochrome *c* release from mitochondria into the cytosol was markedly delayed by GluR2 overexpression. Cytosolic (15 μg) and crude mitochondrial (2 μg) fractions from the lumbar spinal cords were immunoblotted. Hsp60 was used as a marker protein for mitochondria. The anti-SOD1 antibody used in this paper recognizes both human (upper band, 22 kDa) and mouse (lower band, 16 kDa) SOD1. † $P < 0.05$, in comparison of S and GS littermates. (**B**) Induction of *cox-2* transcription was significantly delayed by GluR2 overexpression. RT–PCR analysis was performed using total RNA extracted from lumbar spinal cords. To confirm exponential amplification in each PCR condition, results using two dilution series of template, which differed in concentration by an order of magnitude, are shown. Significance of difference was assessed from the results using larger amounts of templates. † $P < 0.05$ and ‡ $P < 0.01$ (S versus GS). (**C**) Astrogliosis was prominent in 8-month-old S, but was barely detected in GS littermates at the same age. The lumbar regions of mouse spinal cords were immunostained with anti-GFAP antibody.

## DISCUSSION

### Motoneuronal $Ca^{2+}$-permeable AMPA receptors contribute to selective cell death in SOD1-related ALS

The present study demonstrates that motoneuronal $Ca^{2+}$-permeable AMPA receptors contribute to the development of SOD1-related ALS. Reducing permeability by motoneuron-preferential GluR2 overexpression significantly prolongs the lifespan of ALS mice by delaying disease onset (Fig. 2B and C). The mutant SOD1 protein level in the ventral spinal cord was not significantly different between S and GS littermates (Supplementary Material, Fig. S2), and *GluR2* mRNA level in spinal motoneurons did not significantly change during the course of disease in *hSOD1*$^{G93A}$ mice (data not shown). Thus, the beneficial effects of GluR2 overexpression do not result from either a reduction of mutant SOD1 expression or a simple compensation of decreased GluR2 expression, but from reduced $Ca^{2+}$-influx through motoneuronal AMPA receptors.

A recent study on chimeric mice between wild-type and mutant SOD1 transgenic mice revealed that the death of motoneurons expressing mutant SOD1 can be delayed when the surrounding non-neuronal cells do not express mutant SOD1 (39). This finding indicates that motoneuronal death triggered by mutant SOD1 is not cell-autonomous, but also depends on the interactions with surrounding glial cells expressing mutant SOD1. However, there must be a reason why only motoneurons die among the neurons surrounded by non-neuronal cells expressing mutant SOD1. The present study provides evidence that the expression of $Ca^{2+}$-permeable AMPA receptors confers a critical feature on motoneurons such that they undergo death in response to mutant SOD1 effects within themselves and surrounding cells.

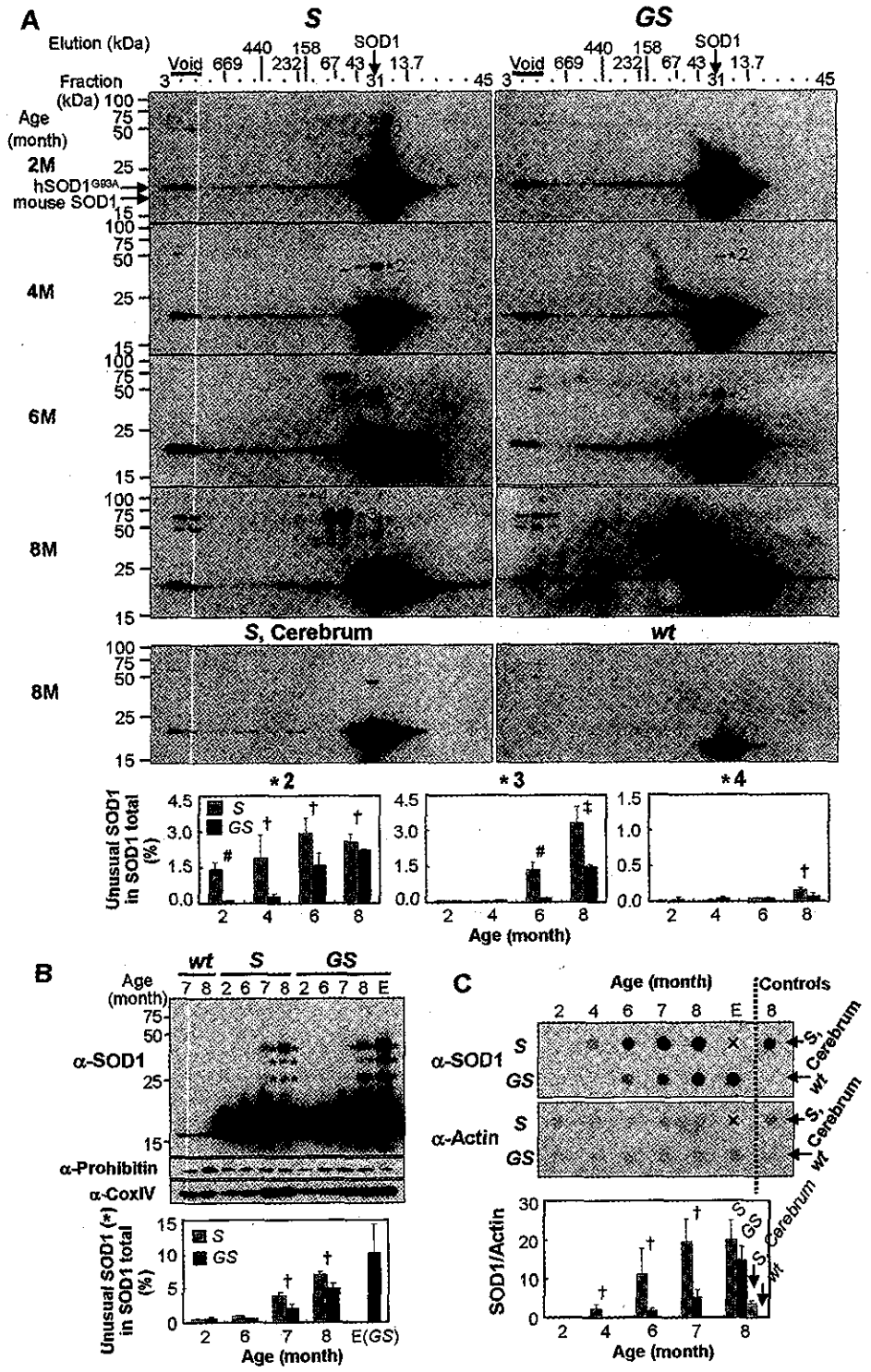


**Figure 4.** Distinctive patterns of unusual SOD1 species are found in the fractions derived from the cytosol and organelle/cytoskeleton, the formation of which is markedly delayed by GluR2 overexpression. (**A**) A very small population of SOD1 proteins is converted into oligomer-sized species in the cytosol long before disease onset, which was effectively delayed by GluR2 overexpression. HPLC fractions derived from ~100 μg of post-mitochondrial (cytosolic protein-enriched) fractions were immunoblotted. Formation of unusual SOD1 species corresponding to a dimer (*2), a trimer (*3) and a tetramer (*4) in size was significantly delayed in GS compared with S littermates. † $P < 0.05$, ‡ $P < 0.01$ and # $P < 0.001$. Non-specific bands appear in the void fraction. (**B**) Unusual SOD1 species differing from those in post-mitochondrial fractions were detected in crude mitochondrial (organelle/cytoskeleton-enriched) fractions at disease onset, which was effectively delayed by *GluR2 overexpression. The crude mitochondrial* fractions (5 μg) were immunoblotted. Asterisks indicate usual SOD1 species corresponding to a dimer, ~25 and 35 kDa sizes. † $P < 0.05$ (S versus GS littermates). (**C**) Filter-trapped SOD1, which might represent misfolded or aggregated forms, increased markedly before disease onset in S, but very slowly in GS littermates. Aliquots 12.5 μg of the post-mitochondrial fractions were solubilized with TBST (0.025% Tween-20) and filtered using cellulose acetate membrane (0.2 μm diameter) followed by immunostaining (10). † $P < 0.05$ (S versus GS littermates).

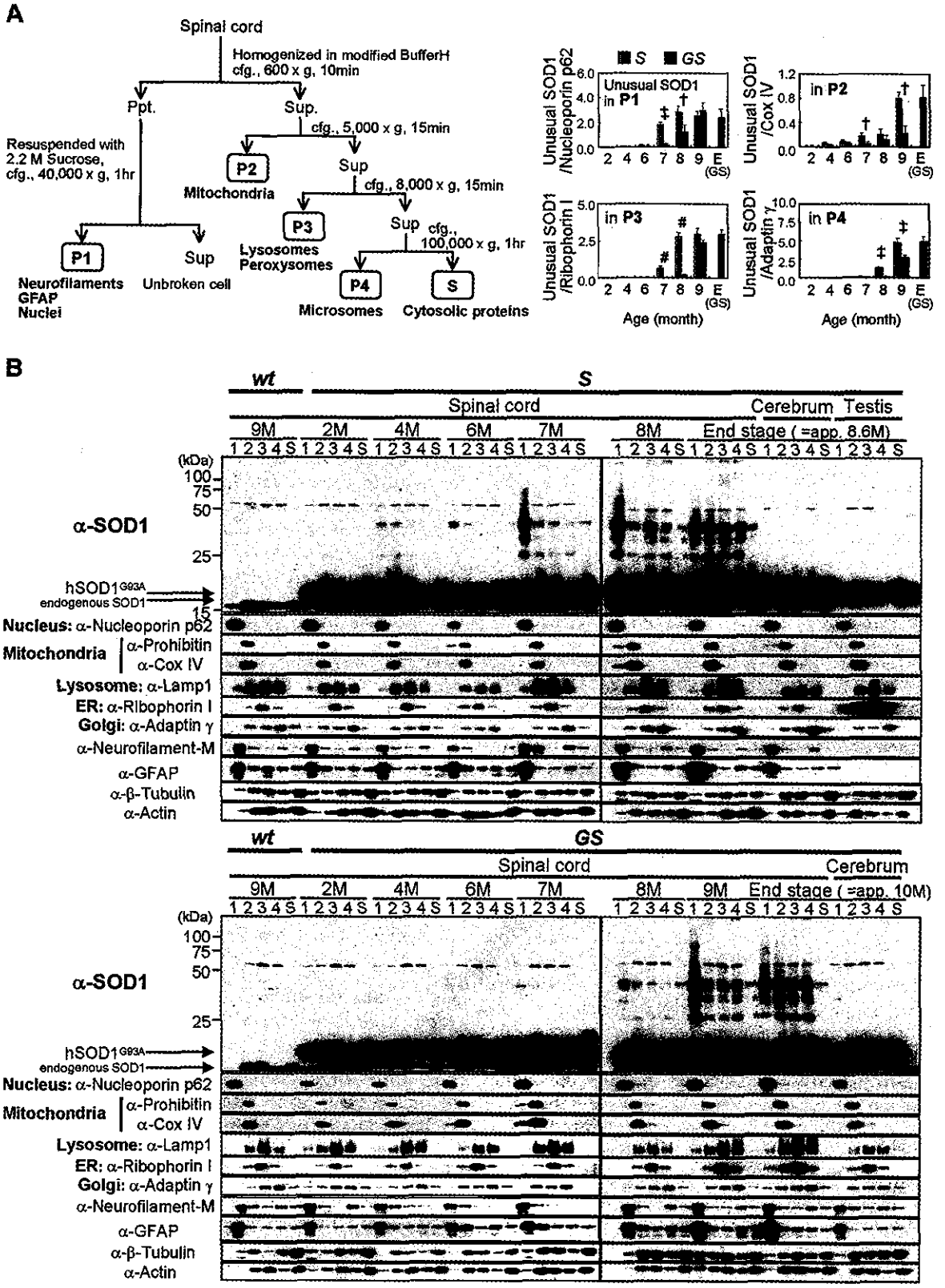


**Figure 5.** Unusual SOD1 species first appear in the fraction enriched in neurofilaments, GFAP, nuclei and mitochondria, which is markedly delayed by GluR2 overexpression. (**A**) The procedure for subcellular fractionation. The representative organelles and cytoskeletons enriched in each fraction are indicated. (**B**) Unusual SOD1 species (asterisks) were first detected in P1 and P2 before disease onset, and then accumulated in other organelle fractions with disease progression. Aliquots of 5 μg of each fraction was immunoblotted. The distribution of each organelle and cytoskeletons was evaluated using antibodies for each marker protein. Accumulation of unusual SOD1 species in spinal cords was significantly delayed in GS compared with S littermates. † $P < 0.05$, ‡ $P < 0.01$ and # $P < 0.001$ (S versus GS littermates).